Mycobacterial Serine/Threonine phosphatase PstP is phospho-regulated and localized to mediate control of cell wall metabolism

Farah Shamma[1], **E. Hesper Rego**[2] **and Cara Boutte** [1*]

[1]Department of Biology, University of Texas at Arlington, Arlington, Texas

[2] Department of Microbial Pathogenesis, Yale University School of Medicine, New Haven, Connecticut

***Corresponding author, cara.boutte@uta.edu**

Key Words: PstP, CwlM, FhaA, Wag31, phospho-regulation, peptidoglycan metabolism, Serine/Threonine Phosphatase

Abstract

The mycobacterial cell wall is profoundly regulated in response to environmental stresses, and this regulation contributes to antibiotic tolerance. The reversible phosphorylation of different cell wall regulatory proteins is a major mechanism of cell wall regulation. Eleven Serine/Threonine protein kinases (STPKs) phosphorylate many critical cell wall-related proteins in mycobacteria. PstP is the sole serine/ threonine phosphatase, but few proteins have been verified as PstP substrates. PstP is itself phosphorylated but the role of its phosphorylation in regulating its activity has been unclear. In this study we aim to discover novel substrates of PstP in *Mycobacterium tuberculosis* (*Mtb*). We show *in vitro* that PstP dephosphorylates two peptidoglycan regulators of *Mtb*, FhaA and Wag31. We also show that a phospho-mimetic mutation of T137 on PstP negatively regulates its catalytic activity against the cell wall regulatory substrates FhaA, Wag31, CwlM, PknB and PknA, and that the corresponding mutation in *Mycobacterium smegmatis (Msmeg)* causes mis-regulation of peptidoglycan *in vivo*. We show that PstP is localized to the septum, which likely restricts its access to certain substrates. These findings on the regulation of PstP provide insight into the control of cell wall metabolism in mycobacteria.

Introduction

Mycobacterium tuberculosis (*Mtb*), which causes Tuberculosis (TB), remains the age-old menace, infecting about 10 million and killing at least a million people worldwide each year (World Health Organization, 2021). TB infections require extended multi-drug antibiotic treatment regimens (Nguyen, 2016). The mycobacterial cell wall contributes to *Mtb*'s inherent antibiotic tolerance (Jarlier and Nikaido, 1994; Sarathy *et al.*, 2013; Batt *et al.*, 2020). The cell wall consists of a covalently linked peptidoglycan-arabinogalactan-mycolic acid layer core surrounding the plasma membrane (Marrakchi *et al.*, 2014). Peptidoglycan is a network of glycan chains cross-linked by small peptides, and is the innermost layer of the wall (Abrahams and Besra, 2021). The wall serves as permeability

43 barrier (Jarlier and Nikaido, 1990; Hett and Rubin, 2008; Hoffmann *et al.*, 2008;
44 Sarathy *et al.*, 2013), and is strongly regulated in response to environmental
45 stresses (Cunningham and Spreadbury, 1998; Betts *et al.*, 2002; Bhamidi *et al.*,
46 2012; Sarathy *et al.*, 2013), including infection (Sharma *et al.*, 2006; Doerks *et*
47 *al.*, 2012). The cell wall changes in response to environmental stresses, and
48 these changes correlate with increased antibiotic tolerance (Xie *et al.*, 2005; Liu
49 *et al.*, 2016; Sarathy *et al.*, 2017). The expression and activity of many cell wall
50 enzymes and regulators are also tightly coordinated over the course of the cell
51 cycle in order to maintain cell wall integrity during elongation and division (Kieser
52 and Rubin, 2014; Dulberger *et al.*, 2020; Bandekar *et al.*, 2020).

53 A crucial regulatory mechanism for transmission of environmental signals to
54 control cell growth is reversible Serine/Threonine (S/T) phosphorylation of a
55 myriad of proteins (Wang *et al.*, 1998; Juris *et al.*, 2000; Echenique *et al.*, 2004).
56 *Mtb* regulates cell physiology and growth (Kang *et al.*, 2005; Gee *et al.*, 2012;
57 Baer *et al.*, 2014; Boutte *et al.*, 2016) through 11 Serine/Threonine kinases
58 (STPKs) (PknA-B and PknD-L) and one essential S/T protein phosphatase PstP
59 (Cole *et al.*, 1998; Bach *et al.*, 2009). PstP is also essential in *Msmeg* (Sharma *et*
60 *al.*, 2016; DeJesus *et al.*, 2017).

61 PstP belongs to the protein phosphatase 2C (PP2C) subfamily of the strictly
62 divalent metal-ion dependent protein serine/threonine phosphatases (Cohen,
63 1989; Barford, 1996; Chopra *et al.*, 2003), known to regulate prokaryotic and
64 eukaryotic cell growth and division, sporulation, stress response and metabolic
65 processes by responding to various environmental signals (Vijay *et al.*, 2000:2;
66 Irmler and Forchhammer, 2001; Mougous *et al.*, 2007; Lu and Wang, 2008;
67 Bradshaw and Losick, 2015; Bradshaw *et al.*, 2017). $PstP_{Mtb}$ shares structural
68 architecture and conserved catalytic residues with the human PP2Cα (Pullen *et*
69 *al.*, 2004) (Figure 1), which is considered the prototypical member of the PP2C
70 family. The N-terminal cytoplasmic enzymatic domain of $PstP_{Mtb}$ (Figure 1)
71 connects to its C-terminal extracellular domain via a transmembrane helix (Pullen
72 *et al.*, 2004). $PstP_{Mtb}$ is itself phosphorylated on T134, T141, T174 and T290

73 (Figure 1) and its phosphorylation affects its activity against small molecule
74 substrates *in vitro* (Sajid *et al.*, 2011) and cell wall metabolism *in vivo* (Shamma
75 *et al.*, 2021).

76 Two essential STPKs, PknA and PknB, play important roles in cell wall regulation
77 by phosphorylating enzymes or regulatory proteins involved in cell division and
78 growth (Sassetti and Rubin, 2003; Kang *et al.*, 2005; Fernandez *et al.*, 2006;
79 Kusebauch *et al.*, 2014; Boutte *et al.*, 2016). Phosphorylation of different cell wall
80 substrates has different effects on their activities. For example, phosphorylation
81 activates synthesis of peptidoglycan precursors through regulatory protein CwlM
82 (Boutte *et al.*, 2016), and inhibits synthesis of mycolic acids by inactivating
83 several mycolic acid biosynthesis enzymes in *Mtb* (Molle *et al.*, 2006; Molle and
84 Kremer, 2010; Veyron-Churlet *et al.*, 2010; Khan *et al.*, 2010; Slama *et al.*, 2011;
85 Vilchèze *et al.*, 2014). PstP is suggested to be a global negative regulator of
86 STPK-mediated phosphorylation (Iswahyudi *et al.*, 2019). Being the only S/T
87 protein phosphatase (Cole *et al.*, 1998), it seems likely to dephosphorylate many
88 of the substrates phosphorylated by the 11 STPKs (Prisic and Husson, 2014).
89 However, only a few proteins have been identified to be substrates of PstP. The
90 biochemically-verified cell wall substrates of PstP include the STPKs PknA and
91 PknB (Boitel *et al.*, 2003; Chopra *et al.*, 2003; Durán *et al.*, 2005; Sajid *et al.*,
92 2011), KasA and KasB, enzymes of the fatty acid synthase –II (FAS-II) system
93 of mycolic acid biosynthesis (Molle *et al.*, 2006), the arabinogalactan layer
94 regulator EmbR (Sharma *et al.*, 2006), and CwlM, which regulates the
95 peptidoglycan layer (Shamma *et al.*, 2021).

96 CwlM is crucial for peptidoglycan synthesis; it interacts with MurA (Boutte *et al.*,
97 2016), the first enzyme of peptidoglycan precursor synthesis (Marquardt *et al.*,
98 1992), and CwlM's phosphorylation is required for MurA's activity (Boutte *et al.*,
99 2016). So dephosphorylation of CwlM~P by PstP (Shamma *et al.*, 2021) should
100 halt peptidoglycan synthesis. Phosphorylated CwlM~P also interacts with FhaA
101 (Turapov *et al.*, 2018), which is involved in modulating peptidoglycan
102 biosynthesis (Gee *et al.*, 2012; Viswanathan *et al.*, 2015; Viswanathan *et al.*,

103 2017) and unphosphorylated CwlM interacts with the peptidoglycan precursor
104 lipid-II flippase MurJ (Turapov *et al.*, 2018), suggesting that CwlM's activity and
105 interactions with other peptidoglycan regulators and enzymes are phospho-
106 regulated and that both CwlM and FhaA are part of a phosphorylation-controlled
107 peptidoglycan regulatory hub (Turapov *et al.*, 2018).

108 FhaA and Wag31 are both regulators of mycobacterial cell wall metabolism.
109 FhaA helps maintain cell envelope integrity, cell length and antibiotic tolerance
110 (Viswanathan *et al.*, 2015; Viswanathan *et al.*, 2017). Available data suggest that
111 FhaA binds and inhibits the MurJ flippase (Gee *et al.*, 2012) and stabilizes PbpA
112 (Viswanathan *et al.*, 2017). FhaA is phosphorylated by PknB (Grundner *et al.*,
113 2005; Prisic *et al.*, 2010; Roumestand *et al.*, 2011), though the role of its
114 phosphorylation in regulation is not yet clear. Wag31 localizes at the cell poles
115 (Kang *et al.*, 2005), is essential for polar peptidoglycan synthesis (Kang *et al.*,
116 2008; Jani *et al.*, 2010) and is phosphorylated by the STPK PknA (Kang *et al.*,
117 2005). Experiments with phospho-mimetic and phospho-ablative mutations of
118 *wag31*T73 suggest that its phosphorylation has a role in controlling
119 peptidoglycan metabolism (Jani *et al.*, 2010). It was not known whether FhaA
120 and Wag31 were actively dephosphorylated, or if their phosphorylated forms
121 were removed through protein degradation.

122 In this study we show that $FhaA_{Mtb}$ and $Wag31_{Mtb}$ are substrates of $PstP_{Mtb}$ *in*
123 *vitro*, and that PstP dephosphorylates Wag31 much faster than it does FhaA or
124 CwlM. PstP's activity against different substrates could be controlled by its
125 localization, by its own phosphorylation (Sajid *et al.*, 2011) or through interactions
126 with other regulatory proteins. Here, we show that the T137E phospho-mimetic
127 mutation of $PstP_{Mtb}$ inhibits $PstP_{Mtb}$'s catalytic activity against the substrates
128 CwlM, FhaA, Wag31, PknB and PknA *in vitro*. Furthermore, the corresponding
129 phospho-mimetic mutation in *Msmeg* leads to dis-regulation of PG metabolism.
130 We also find that PstP is enriched at the cell division site, suggesting that its
131 access to substrates at the pole might also control its activity. We suggest a
132 model where PstP's activity against assorted substrates is regulated by substrate

133 affinity and protein localization, and further toggled by the phosphorylations on
134 PstP.

135 **Methods and Materials**

136 **Bacterial strains and culture conditions**

137 All *Mycobacterium smegmatis* mc^{2}155 ATCC 700084 cultures were grown in 7H9
138 (Becton, Dickinson, Franklin Lakes, NJ) medium containing 0.003 g/liter catalase,
139 5 g/liter bovine serum albumin (BSA), 2 g/liter dextrose, 0.2% glycerol, 0.85
140 g/liter NaCl, and 0.05% Tween 80 and incubated at 37°C until log. phase. 1xPBS
141 supplemented with 0.05% Tween 80 was used for starvation assays. Cultures
142 were plated on LB Lennox agar (Fisher BP1427-2).

143 *E. coli* Top10, XL1-Blue, and Dh5α strains were used for cloning and *E. coli* BL21
144 Codon Plus and BL21(DE3) strains were used for expressing proteins. Antibiotic
145 concentrations for *M. smegmatis* were 25µg/ml kanamycin and 20 µg/ml zeocin.
146 Antibiotic concentrations for *E. coli* were 50 µg/ml kanamycin, 25 µg/ml zeocin,
147 20 µg/ml chloramphenicol, and 140 µg/ml ampicillin.

148 **Cloning and Strain construction**

149 N-terminally Histidine (His) tagged cytosolic domains (1-300 amino acids (Gupta
150 *et al.*, 2009)) of *pstP*$_c$T137E$_{Mtb}$ and *pstP*$_c$T141E$_{Mtb}$, and *fhaA*WT$_{Mtb}$ codon-
151 optimized for expression in *E. coli* were ordered from IDT, Inc. and cloned in to
152 pET28a.

153 The *Msmeg* mc^{2}155 strains Δ*pstP*::lox L5::pCT94-p766tetON6-*pstP*$_{Msmeg}$T134E
154 and Δ*pstP*::lox L5::pCT94-p766tetON6-*pstP*$_{Msmeg}$WT were generated by L5 allele
155 swapping as described previously (Pashley and Parish, 2003; Shamma *et al.*,
156 2021). All vectors and strains are described in supplementary tables 1-3.

157 A vector that expressed mCherry-2B-PstP$_{Msmeg}$ was constructed using isothermal
158 assembly and integrated at the tweety phage integration site in *Msmeg*. In brief,

159 *pstP* was amplified from *Msmeg* genomic DNA, and subcloned into a plasmid
160 along with *mCherry2B* and the uv15 ribosomal promoter. The resulting vector
161 was transformed into *Msmeg*.

162 **Growth Curve Assay**

163 At least three biological replicates of $pstP_{Msmeg}$T134E and WT allelic variants
164 were grown in 7H9 medium up to the mid-log. phase. The growth curve assays
165 were performed in non-treated non-tissue culture plates using a plate reader
166 (BioTek Synergy neo2 multi mode reader) in 200µl of 7H9 medium at 37°C
167 starting at an Optical Density at 600nm (OD_{600}) of 0.1.

168 The doubling times of each strain were calculated in the non-linear (curve fit)
169 method using an exponential growth equation with the least squares (ordinary) fit
170 in GraphPad Prism (version 7.0d). *P* values were calculated using two-tailed
171 unpaired t-tests.

172 **Protein purification**

173 His-MBP-$PknA_{Mtb}$ was expressed in *E. coli* BL21(DE3) and all other proteins were
174 expressed using *E. coli* BL21 Codon Plus cells. The *Mtb* genes of all studied
175 factors were cloned into expression vectors. His-MBP-$PknB_{Mtb}$, His-SUMO-
176 $CwlM_{Mtb}$, His-$PstP_cWT_{Mtb}$ and His-$PstP_cT174E_{Mtb}$ were expressed and purified as
177 previously described (Kieser *et al.*, 2015; Shamma *et al.*, 2021). His-
178 $PstP_cT137E_{Mtb}$ and His-$PstP_cT141E_{Mtb}$ were expressed and purified using the
179 same conditions and buffers used to purify His-$PstP_cWT_{Mtb}$ and His-
180 $PstP_cT174E_{Mtb}$ (Shamma *et al.*, 2021).

181 His-$Wag31_{Mtb}$ was induced with 0.5mM IPTG (isopropyl-*β*-D-
182 thiogalactopyranoside) for 6h at 18°C, and purified on Ni-NTA resin (G-
183 Biosciences 786-940) then dialyzed and concentrated. The buffer for His-
184 $Wag31_{Mtb}$ was 50mM Tris pH 8, 350mM NaCl, 1 mM dithiothreitol (DTT), and

185 10% glycerol. Imidazole (10mM and 20mM) was added to the buffers for lysis of
186 the cell pellets and washing the Ni-NTA resin respectively, and 250mM imidazole
187 was added for elution. The lysis buffer was supplemented with 1mM PMSF and
188 0.2% Triton X100.

189 His-MBP-PknA$_{Mtb}$ (1-279 amino acids containing the kinase domain (Baer *et al.*,
190 2014)) was induced with 0.5mM IPTG at 18°C overnight, purified with 5ml Ni-
191 NTA resins (BIO-RAD EconoFit Nuvia IMAC, 12009287), then run over the size
192 exclusion resin (Enrich SEC650, BIO-RAD 780-1650) after dialysis and
193 concentration to get soluble protein. The buffer for purifying His-MBP-PknA$_{Mtb}$
194 was 50mM Tris pH 7.5, 150mM NaCl, 20% glycerol. PMSF (1mM) was added to
195 the buffer while resuspending the cell pellets. Imidazole was used in buffer for
196 application to (20mM) and for elution from Ni-NTA resin (200mM).

197 His-FhaA$_{Mtb}$ was induced with 1mM IPTG at 18°C overnight and purified on Ni-
198 NTA resin (G-Biosciences, 786-940 in 5 ml Bio-Scale Mini Cartridges, BIO-RAD
199 7324661), then dialyzed, concentrated, and run over size exclusion resin (GE
200 Healthcare Sephacryl S-200 in HiPrep 26/70 column). His-FhaA$_{Mtb}$ was purified
201 using the buffers described in (Roumestand *et al.*, 2011).

202 ***In vitro* dephosphorylation assays**

203 His-SUMO-CwlM$_{Mtb}$ at 0.15 µg/µl was phosphorylated *in vitro* with His-MBP-
204 PknB$_{Mtb}$ at 0.015 µg/µl for 30 minutes at room temperature with 0.15µCi/µl ATP
205 [γ-^{32}P] (3000Ci/mmol, 10mCi/ml, PerkinElmer BLU002A250UC) and 2mM $MnCl_2$ in
206 buffer (50mM Tris, pH 7.5, 250mM NaCl, 10% glycerol and 1mM DTT). Right
207 after collecting kinase reaction samples, the leftover mixture was split into equal
208 parts in different microcentrifuge tubes to carry on phosphatase assays by
209 adding replicates of His-PstP$_c$WT$_{Mtb}$, His-PstP$_c$T137E$_{Mtb}$, His-PstPcT141E$_{Mtb}$ or
210 His-PstPcT174E$_{Mtb}$ at 0.012 µg/µl to the kinase reaction mixtures containing 0.12
211 µg/µl of His-SUMO-CwlM$_{Mtb}$ and incubated in phosphatase buffer (50mM Tris pH
212 7.5, 10mM $MnCl_2$, and 1mM DTT) at room temperature up to 40 minutes. His-

213 $FhaA_{Mtb}$ at 0.15 µg/µl was phosphorylated *in vitro* with His-MBP-$PknB_{Mtb}$ at 0.015
214 µg/µl for 45 minutes at 37°C with 0.15µCi/µl ATP [γ-^{32}P] in presence of 5mM
215 $MnCl_2$ in 25mM Tris pH 7.5 and 1mM DTT. Right after collecting 0 minute kinase
216 reaction sample, the reaction mixture was then split into equal parts and
217 incubated with either $PstP_cWT_{Mtb}$ or different phospho-mimetic variants of it at
218 0.012 µg/µl up to 80 minutes at room temperature in presence of the
219 phosphatase buffer where the concentration of the substrate was 0.12 µg/µl For
220 CwlM and FhaA, the amount of kinase and phosphatases was 1/10th the amount
221 of substrate, by weight.

222 His-$Wag31_{Mtb}$ at 0.15 µg/µl was phosphorylated with His-MBP-$PknA_{Mtb}$ at 0.03
223 µg/µl for 2 hours at room temperature in presence of 0.2µCi/µl ATP [γ-^{32}P], 10mM
224 $MnCl_2$ and buffer (50mM Tris pH 7.5, 20% glycerol and 150mM NaCl). The amount of
225 PknA was 1/5th the amount of Wag31 substrate, by weight.

226 The kinase reaction mixture was equally split in to separate tubes after the 0
227 second kinase reaction sample was taken. His-$PstP_cWT_{Mtb}$ or its different
228 phospho-mimetic variants at 0.0013 µg/µl were added to the mixture containing
229 0.13 µg/µl substrate and incubated at room temperature for up to 120 seconds in
230 the phosphatase buffer. The amount of phosphatase was 1/100th the amount of
231 Wag31 substrate in the phosphatase reactions, by weight.

232 Control samples with no kinase and with no phosphatase were performed in all
233 the above-mentioned substrate dephosphorylation assays. All *in vitro*
234 dephosphorylation assays were carried out separately with two individually
235 purified batches of WT and phospho-mimetic mutant of PstP as biological
236 replicates.

237 **Quantification of γ-^{32}P signals**

238 Samples from each *in vitro* biochemical reaction were collected before (0 minute
239 or second) and after addition of each of the phosphatases at several different
240 time points. The samples were run on 12% (Mini-Protean TGX, BIO-RAD,

241 4561046) gels and stained with Coomassie blue solution. After destaining, gels
242 were dried using the GD200 Vacuum Gel Drying system (Hoefer Inc.) and
243 imaged with phosphor screens (Molecular Dynamics) and a scanner (Storm 860,
244 Amersham Biosciences). ImageQuant software (Molecular Dynamics) was used
245 to process the images.

246 The protein bands on the gel and the phospho-signals on the autoradiogram
247 were then quantified with FIJI. The intensities of the substrate protein bands on
248 the Coomassie-stained gel and their corresponding phospho-signals on the
249 autoradiograms at each time point were normalized against the respective
250 protein band and the phospho-signal at 0 minute (His-SUMO-CwlM$_{Mtb}$ and His-
251 FhaA$_{Mtb}$) or 0 second (His-Wag31$_{Mtb}$) before addition of the phosphatase. These
252 relative intensities were used to calculate the intensity of phospho-signal over the
253 amount of substrate for each time point. These values were used to plot the
254 graph. The P32 signal intensities of the kinases on autoradiograms at each time
255 point were normalized against the respective phospho-signal on the kinase at 0
256 minute (His-MBP-PknB$_{Mtb}$) or 0 second (His-MBP-PknA$_{Mtb}$) before addition of the
257 phosphatase. These relative P32 signal intensity values were then used to plot
258 the graph. All values were plotted and p-values were calculated using two-tailed,
259 unpaired Student's t-test in GraphPad Prism (version 7.0d).

260 **Cell staining**

261 At least three biological replicates of *pstP*$_{Msmeg}$ T134E and WT allelic variants
262 were grown in 7H9 medium up to mid log. phase. Cultures were washed and
263 then starved in 1xPBS with 0.05% Tween 80 (PBST) at $OD_{600=}$ 0.3 for 15
264 minutes. 100µl of starved culture was then treated with 3µl of 10mM fluorescent
265 D-amino acid HADA for 10 minutes. Cells were then pelleted and resuspended in
266 PBST and fixed with 10µl of 16% paraformaldehyde for 10 minutes at room
267 temperature. Cells were then pelleted and resuspended in PBST before imaging
268 on agarose pads.

269 For staining cells in the log. phase, 1µl of 1mM HADA was added to 100µl
270 culture grown up to the mid-log. phase and incubated at 37°C for 15 minutes.
271 Stained cells were then pelleted, washed and fixed as described above.

272 **Static microscopy and image analysis**

273

274 A Nikon Ti-2 widefield epifluorescence microscope with a Photometrics Prime
275 95B camera and a Plan Apo 100x, 1.45 NA objective lens was used to image
276 cells. A 350/50nm excitation filter and a 460/50nm emission filter were used to
277 take the blue fluorescence images for HADA staining. All images were captured
278 using the NIS Elements software and analyzed using FIJI and MicrobeJ (Ducret
279 *et al.*, 2016). Appropriate parameters for length, width and area were set in
280 MicrobeJ to detect cells. All detected dividing (V-snapping) cells in the images
281 were split at the septum so that each daughter cell could be considered as a
282 single cell. No overlapping cells in the images were included in the analysis.

283

284 Length and mean-intensities of HADA signals of at least 330 cells from each of
285 *pstP*T134E$_{Msmeg}$ and *pstP*WT$_{Msmeg}$ (at least 110 cells from each of three biological
286 replicate strains of each genotype) were quantified using MicrobeJ. The values of
287 the mean intensities of 330 cells of each *pstP* allelic mutant and WT are
288 represented in the graphs generated using GraphPad Prism (version 7.0d).

289

290 The medial intensity profiles of HADA signals in cells from different *pstP* allele
291 strains in log. phase and starvation analyzed with MicrobeJ were plotted on the
292 Y-axis over relative positions of cells using the “XStatProfile” plotting feature in
293 MicrobeJ to show the subcellular localization of fluorescent intensities in cells.
294 Demographs of HADA signal intensity across cell lengths in log. phase and
295 starvation were built using the “Demograph” feature of MicrobeJ by plotting the
296 medial intensity profiles of HADA signals.

297

298 **Time-lapse microscopy**

299

300 An inverted Nikon Ti-E microscope was used for the time-lapse imaging. An
301 environmental chamber was maintained at 37°C. Cells were cultivated in an B04
302 microfluidics plate from CellAsic; continuously supplied with fresh medium; and
303 imaged every 15 minutes using a 60x 1.4 N.A. phase contrast objective, with an
304 intermediate magnification of 1.5x. mCherry2B was excited with a SpectraX
305 Illuminator at 561-nm. Fluorescence was detected with a bandpass filter of
306 595/40 and detected with an ORCA Flash Digital sCMOS.

307

308 **Results**

309

310 **PstP$_{Mtb}$ dephosphorylates FhaA$_{Mtb}$ and Wag31$_{Mtb}$ *in vitro***

311 FhaA$_{Mtb}$ is phosphorylated by PknB$_{Mtb}$ *in vivo* (Prisic *et al.*, 2010) and *in vitro*
312 (Grundner *et al.*, 2005; Roumestand *et al.*, 2011) on T116 (Roumestand *et al.*,
313 2011). Wag31$_{Mtb}$ is phosphorylated at T73 by PknA$_{Mtb}$ (Kang *et al.*, 2005). To
314 determine if FhaA$_{Mtb}$ and Wag31$_{Mtb}$ are substrates of PstP$_{Mtb}$, we performed *in*
315 *vitro* dephosphorylation assays with purified full-length His-FhaA$_{Mtb}$, His-
316 Wag31$_{Mtb}$, N-terminally His-MBP tagged cytosolic kinase domains of PknA$_{Mtb}$ and
317 PknB$_{Mtb}$, and the cytosolic region of PstP$_{Mtb}$ containing the catalytic domain (His-
318 PstP$_c$WT$_{Mtb}$).

319 We phosphorylated His-FhaA$_{Mtb}$ with His-MBP-PknB$_{Mtb}$ and ATP [γ-^{32}P]. After
320 addition of 1/10th the amount of His-PstP$_c$WT$_{Mtb}$, the phosphorylation on His-
321 FhaA$_{Mtb}$~P decreases by ~80% in 80 minutes (Figure 2a,b). Our control assay
322 with no phosphatase shows that the phosphorylation on His-FhaA$_{Mtb}$~P is stable
323 over time in the phosphatase buffer (Figure 2a, b). These data show that the cell
324 wall regulator FhaA$_{Mtb}$ is a substrate of PstPWT$_{Mtb}$ *in vitro*.

325 We performed similar phosphatase assays to determine if PstP$_c$WT$_{Mtb}$ can
326 dephosphorylate Wag31$_{Mtb}$. We first phosphorylated His-Wag31$_{Mtb}$ with His-MBP-

327 PknA$_{Mtb}$ and ATP [γ-^{32}P], then added His-PstP$_c$WT$_{Mtb}$. With 1/100th the amount of
328 PstP compared to Wag31, Wag31$_{Mtb}$ phosphorylation decreased by about ~90%
329 in 2 minutes (Figure 3a,b), only in the presence of His-PstP$_c$WT$_{Mtb}$. These data
330 show that Wag31$_{Mtb}$ is a substrate of PstPWT$_{Mtb}$ *in vitro*.

331 Our previous biochemical data that demonstrated PstP$_{Mtb}$ dephosphorylates
332 CwlM$_{Mtb}$ (Shamma *et al.*, 2021) is reproducible in our *in vitro* assays with ATP [γ-
333 ^{32}P] where we observe a 97% decrease in phosphorylation on His-SUMO-CwlM$_{Mtb}$~P
334 over a time period of 40 minutes after addition of His-PstP$_c$WT$_{Mtb}$ (Figure 4a, b). In all
335 the assays, we see no phosphorylation signals on the WT and phospho-mimetic
336 PstPs on the autoradiograms (data not shown) since PstP can quickly
337 dephosphorylate itself (Sajid *et al.*, 2011) and the purified forms are thus
338 unphosphorylated.

339 Because measuring the rates of dephosphorylation by PstP against different
340 substrates required different PstP concentrations and timing, we calculated the
341 initial linear rate of dephosphorylation per unit concentration of PstP, in order to
342 compare PstP's activity against different substrates. This comparison indicates
343 that His-PstP$_c$WT$_{Mtb}$ dephosphorylates His-Wag31$_{Mtb}$ more than 500 times faster
344 than His-SUMO-CwlM$_{Mtb}$ and about 2500 times faster than His-FhaA$_{Mtb}$ (Figure
345 4c).

346 **Phospho-mimetic mutation at PstPT137$_{Mtb}$ inhibits dephosphatase activity**

347 PstP$_{Mtb}$ is phosphorylated on the conserved threonine (T) residues 137, 141 and
348 174 (Figure 1), and when phosphorylated, shows increased activity against small
349 molecule substrates *in vitro* (Sajid *et al.*, 2011). We hypothesized that
350 phosphorylation of the threonine residues of PstP individually might help regulate
351 PstP's activity through switching its catalytic activity against different substrates
352 or by affecting substrate affinity. To test this, we made phospho-mimetic (T to E)
353 (Cottin *et al.*, 1999) mutants of PstP$_{Mtb}$ at each of the three conserved
354 phosphorylation sites of PstP$_{Mtb}$ in the catalytic domain and purified them (His-

355 PstP$_c$T137E$_{Mtb}$, His-PstP$_c$T141E$_{Mtb}$ and His-PstP$_c$T174E$_{Mtb}$). We previously
356 showed that *in vitro* His-PstP$_c$WT$_{Mtb}$ and His-PstP$_c$T174E$_{Mtb}$ dephosphorylate
357 His-SUMO-CwlM$_{Mtb}$ at the same rate (Shamma *et al.*, 2021). We performed
358 separate *in vitro* phosphatase assays with the substrates His-FhaA $_{Mtb}$, His-
359 Wag31$_{Mtb}$ and His-SUMO-CwlM$_{Mtb}$ with the phospho-mimetic versions of PstP.
360 His-PstP$_c$T137E$_{Mtb}$ is completely inactive *in vitro* against all three substrates
361 (Figures 2,3,4). This suggests that phosphorylation on T137 of PstP may inhibit
362 its activity against multiple substrates.

363 His-MBP-PknB$_{Mtb}$ and His-MBP-PknA$_{Mtb}$, the STPKs used in these assays, are
364 also confirmed substrates of PstP (Sajid *et al.*, 2011). PknA and PknB are
365 activated to phosphorylate their own substrates when they themselves are
366 phosphorylated at their activation loops (Baer *et al.*, 2014). Because we already
367 had these kinases in our phosphatase assays, we were able to measure
368 dephosphorylation of His-MBP-PknB$_{Mtb}$ and His-MBP-PknA$_{Mtb}$ by PstP in the
369 context of a 10-fold and 5-fold excess of His-SUMO-CwlM$_{Mtb}$ or His-Wag31$_{Mtb}$,
370 respectively. We found that His-PstP$_c$T137E$_{Mtb}$ dephosphorylates both His-
371 MBP-PknB$_{Mtb}$ (Figure 5a,b) and His-MBP-PknA$_{Mtb}$ (Figure 5c,d) more slowly than
372 His-PstP$_c$WT$_{Mtb}$ and the other PstP mutants. This shows that His-PstP$_c$T137E$_{Mtb}$
373 is inhibited against at least five different substrates.

374

375 **Phospho-mimetic mutations at PstPT141$_{Mtb}$ and PstPT174$_{Mtb}$ moderately**
376 **inhibit Wag31's dephosphorylation**

377 His-PstP$_c$T141E$_{Mtb}$ and His-PstP$_c$T174E$_{Mtb}$ dephosphorylate His-FhaA$_{Mtb}$ (Figure
378 2,4c) and His-SUMO-CwlM$_{Mtb}$ (Figure 4) at about the same rate as His-
379 PstP$_c$WT$_{Mtb}$, but dephosphorylate His-Wag31$_{Mtb}$ about half as fast as His-
380 PstP$_c$WT$_{Mtb}$ (Figure 3, 4c). These biochemical data support our hypothesis that
381 phosphorylation on PstP may modulate its activity by affecting its substrate
382 specificity. Phosphorylation at T141 and T174 appear to inhibit binding or

383 catalysis of Wag31 but not FhaA or CwlM.

384 **Phospho-site T134 of PstP$_{Msmeg}$ regulates peptidoglycan metabolism in**
385 **starvation**

386 Phosphorylation of CwlM allows it to activate the peptidoglycan precursor
387 enzyme MurA, thereby licensing peptidoglycan synthesis (Boutte *et al.*, 2016).
388 Phosphorylation of CwlM also affects its binding to FhaA and the lipid II flippase
389 MurJ (Turapov *et al.*, 2018). CwlM is quickly dephosphorylated in the transition to
390 stasis (Boutte *et al.*, 2016) likely by PstP (Shamma *et al.*, 2021). The function of
391 phosphorylation on FhaA and Wag31 is not yet clear, but available data (Jani *et*
392 *al.*, 2010; Gee *et al.*, 2012; Viswanathan *et al.*, 2016) suggest it could also affect
393 peptidoglycan metabolism. Dephosphorylation of these regulators could be
394 important for downregulation of peptidoglycan metabolism in stasis.

395 As the phospho-mimetic mutation at PstPT137$_{Mtb}$ inhibits PstP's
396 dephosphorylation of three peptidoglycan regulatory proteins *in vitro* (Figure
397 2,3,4), we sought to determine if the corresponding phosphosite on PstP (T134)
398 might affect peptidoglycan metabolism *in vivo* in *Msmeg*. We made *Msmeg*
399 strains with a phospho-mimetic *pstP*T134E$_{Msmeg}$ allele replacing the wild-type
400 *pstP*. We reported previously that the biological replicates of *pstP*T134E$_{Msmeg}$
401 mutant strains had inconsistent doubling times (Shamma *et al.*, 2021) probably
402 due to potential suppressor mutations. We confirmed that the slow growing
403 clones could, after passaging, accumulate suppressor mutations that allowed
404 them to grow as fast as the *pstP*WT strain. To characterize the original
405 *pstP*T134E$_{Msmeg}$ strain, we isolated numerous clones from fresh transformations,
406 and measured the doubling times of each before continuing with experiments.
407 We show data only from clones that grew at the slower rate.

408 We used three biological replicate *pstP*T134E$_{Msmeg}$ strains that had consistently
409 slower growth than the *pstP*WT$_{Msmeg}$ strains (Figure 6a, red bar) in our next
410 experiments. We stained both log.phase and starved *pstP* T134E$_{Msmeg}$ and

411 WT_{Msmeg} strains using a fluorescent D-amino acid HADA (Kuru *et al.*, 2012) as a
412 reporter of active peptidoglycan metabolism. We saw a slight increase in length
413 (Figure 6b,d and Supplementary Figure S2a,b) and HADA intensity (Figure 6c,d
414 and Supplementary Figure S2a,b) in the *pstP* $T134E_{Msmeg}$ strains in the log.
415 phase compared to the WT_{Msmeg} strains. After starvation, these differences
416 increased (Figure 6b,c,e and Supplementary Figure S2c,d). WT_{Msmeg} strains
417 quickly downregulate peptidoglycan metabolism upon starvation (Boutte *et al.*,
418 2016), as the decreased HADA staining (Figure 6c,d,e,f,g) shows. The starved
419 *pstP*$T134E_{Msmeg}$ strains show significantly higher HADA signal than the WT_{Msmeg}
420 (Figure 6c, top right panels of d,e and Supplementary Figure S2b,d) indicating a
421 defect in downregulating peptidoglycan metabolism. This suggests that the
422 presence of a constant negative charge on phosphosite T134 of $PstP_{Msmeg}$
423 impairs downregulation of peptidoglycan synthesis, likely by inhibiting PstP's
424 dephosphorylation of peptidoglycan regulators (Figure 2,3,4).

425 Our data showing that the *pstP*$T134E_{Msmeg}$ strains have increased length (Figure
426 6b) and higher HADA intensity (Figure 6c,d,f and Supplementary Figure S2b) in
427 the log. phase support the notion (Jani *et al.*, 2010; Turapov *et al.*, 2018) that
428 peptidoglycan regulation involves a balance in phosphorylated and
429 dephosphorylated forms of its regulatory substrates and PstP's phospho-
430 regulation helps toggle its activity against substrates in log. phase. The
431 misregulation of peptidoglycan metabolism (Figure 6c,d,e,f,g and Supplementary
432 Figure S2b,d) may account for the slower growth of the *pstP*$T134E_{Msmeg}$ strains
433 that we see in our data (Figure 6a), though it is likely that other processes
434 beyond peptidoglycan metabolism are also misregulated, as PstP likely has
435 many substrates involved in diverse processes (Molle *et al.*, 2006; Iswahyudi *et*
436 *al.*, 2019).

437

438

439 **PstP localizes at the septum in exponentially growing *Msmeg* cells**

440 We sought to determine if PstP's activity against its diverse substrates could be
441 regulated through protein localization. We made an *Msmeg* strain carrying an
442 additional copy of $pstP_{Msmeg}$ fused to *mCherry2B*. By time-lapse fluorescence
443 microscopy, we observed that mCherry2B-$PstP_{Msmeg}$ appears to be uniformly
444 distributed along the membrane throughout most of the cell cycle, but becomes
445 localized at the septum before cell separation (Figure 7). These data suggest that
446 PstP is also regulated by its access to substrates at different sites in the cell.

447 **Discussion**

448 Previous works have suggested that PstP plays a crucial role as a negative
449 regulator of protein Serine/ Threonine phosphorylation (Boitel *et al.*, 2003; Molle
450 *et al.*, 2006; Sajid *et al.*, 2011; Boutte *et al.*, 2016; Iswahyudi *et al.*, 2019;
451 Dulberger *et al.*, 2020; Shamma *et al.*, 2021). Our findings indicate that PstP is
452 regulated by its own phosphorylation (Figure 2,3,4,5) to regulate cell wall
453 metabolism (Figure 6), and that it may also be regulated by its localization
454 (Figure 7).

455 We see that $PstPWT_{Mtb}$ dephosphorylates $CwlM_{Mtb}$, $FhaA_{Mtb}$ and $Wag31_{Mtb}$ at
456 different rates *in vitro* (Figure 4c), with $Wag31_{Mtb}$ being the fastest to be
457 dephosphorylated and FhaA the slowest (Figure 4c). We showed that PstP
458 localizes at the septum in the exponentially growing *Msmeg* cells (Figure 7). Both
459 FhaA and Wag31 localize at the poles and septum (Gee *et al.*, 2012; Hannebelle
460 *et al.*, 2020). Our localization data (Figure 7) suggest that both Wag31 and FhaA
461 (Figure 2, 3, 4c) may be more highly phosphorylated at the poles than at the
462 septum. PstP's rapid dephosphorylation of Wag31 (Figure 3, 4c) suggests that it
463 is likely to be nearly completely unphosphorylated at the septum.

464 Our data in Figure 2, 3 and 4 show that negative charges at $PstPT141_{Mtb}$ and
465 $T174_{Mtb}$ slow dephosphorylation of $Wag31_{Mtb}$, but not $FhaA_{Mtb}$ and $CwlM_{Mtb}$.
466 Phosphorylation site T141 is on the flap subdomain and T174 is on the β-sheet

467 core (β8) on PstP$_{Mtb}$ (Pullen *et al.*, 2004), but both are facing into the same
468 groove between these domains (Figure 1). T137 is the first residue of the flap
469 subdomain (Pullen *et al.*, 2004), and it faces away from the groove with the other
470 phospho-sites (Figure 1). We propose that the T141/ T174 groove may contribute
471 to toggling specificity of PstP against certain substrates, depending on the
472 phosphorylation status.

473 Our *in vitro* data in Figure 2,3, 4 and 5 show that PstPT137E$_{Mtb}$ inhibits its activity
474 against CwlM$_{Mtb}$, FhaA$_{Mtb}$ and Wag31$_{Mtb}$, and also against the STPKs PknA and
475 PknB that phosphorylate them, all of which are involved in regulation of
476 peptidoglycan metabolism (Thakur and Chakraborti, 2006; Kang *et al.*, 2008; Jani
477 *et al.*, 2010; Gee *et al.*, 2012; Prisic and Husson, 2014; Boutte *et al.*, 2016;
478 Viswanathan *et al.*, 2016; Viswanathan *et al.*, 2017; Carette *et al.*, 2018; Turapov
479 *et al.*, 2018). We expected the corresponding phospho-mimetic mutant
480 *pstP*T134E$_{Msmeg}$ allele to cause mis-regulation of peptidoglycan synthesis *in vivo*.
481 Our *in vivo* data show that the *pstP*T134E$_{Msmeg}$ strains grow more slowly, and
482 have an increase in cell length and HADA staining in log. phase and starvation
483 (Figure 6). We see relatively mild defects in peptidoglycan metabolism in these
484 strains in log. phase (Figure 6b,c), which suggests that phospho-site T134 on
485 PstP may not be important for controlling peptidoglycan metabolism in active
486 growth. Alternatively, the function of the negative charge at T134 may be
487 different in the cell: phosphorylation here could help recruit an interacting protein
488 that could alter PstP's activity in a different way. As expected, however, we do
489 see greater defects in peptidoglycan metabolism during starvation (Figure
490 6c,d,e,f,g), suggesting that dephosphorylation of CwlM, FhaA, Wag31, PknB or
491 PknA, and/or other substrates, is more important in the transition to stasis than in
492 log. phase. The cells still largely downregulate peptidoglycan metabolism,
493 indicating that other regulatory systems contribute to this response, or that
494 *pstP*T134E has different effects *in vivo* than *in vitro*.

495 Although our findings are limited to PstP's activity on certain substrates only,
496 altogether they prove that the individual phosphosites are important in regulating

497 PstP. *In vitro*, we see that a negative charge on T137 of $PstP_{Mtb}$ inhibits its
498 activity against three PG regulators (Figure 2,3,4), as well as the essential
499 kinases PknB and PknA when they are mixed together (Figure 5). In the cell, the
500 substrates and kinases also co-exist, and PstP may exert its effect directly by
501 dephosphorylating the substrates or indirectly by acting on the kinase (Bhaskara
502 *et al.*, 2019), or both simultaneously. There are likely other mechanisms of cell
503 wall regulation involved in the complex *in vivo* scenario like protein localization or
504 PstP's interaction with other regulatory proteins that may contribute to PstP's
505 regulation as well. We do not know the conditions under which PstP is
506 phosphorylated, or the combinations of PstP's phosphorylations that exist in the
507 cell. So the *in vitro* data may not mirror the deep complexity of the STPK-
508 substrate-PstP network *in vivo*.

509 In this work we show that PstP is regulated by both phosphorylation and
510 localization. This work demonstrates the importance of protein
511 dephosphorylation, not just phosphorylation, in regulating the activity of proteins
512 involved in cell wall metabolism in mycobacteria. Future work that addresses
513 when all of these important phospho-sites are phosphorylated and
514 dephosphorylated will help us to understand how all these protein regulators
515 contribute to coordinating the construction and integrity of the cell wall in
516 changing conditions.

517 **Acknowledgement:**

518 This work was supported by NIH grant R01AI148917 to CCB and R01AI148255
519 to EHR.

520

521

522

523

524

525 **References:**

526 Abrahams, K.A., and Besra, G.S. (2021) Synthesis and recycling of the mycobacterial
527 cell envelope. *Current Opinion in Microbiology* **60**: 58–65
528 https://linkinghub.elsevier.com/retrieve/pii/S1369527421000187. Accessed February 17,
529 2022.

530 Bach, H., Wong, D., and Av-Gay, Y. (2009) Mycobacterium tuberculosis PtkA is a novel
531 protein tyrosine kinase whose substrate is PtpA. *Biochemical Journal* **420**: 155–162
532 https://portlandpress.com/biochemj/article/420/2/155/44900/Mycobacterium-
533 tuberculosis-PtkA-is-a-novel-protein. Accessed November 15, 2021.

534 Baer, C.E., Iavarone, A.T., Alber, T., and Sassetti, C.M. (2014) Biochemical and Spatial
535 Coincidence in the Provisional Ser/Thr Protein Kinase Interaction Network of
536 *Mycobacterium tuberculosis*. *J Biol Chem* **289**: 20422–20433
537 http://www.jbc.org/lookup/doi/10.1074/jbc.M114.559054. Accessed October 23, 2019.

538 Bandekar, A.C., Subedi, S., Ioerger, T.R., and Sassetti, C.M. (2020) Cell-Cycle-
539 Associated Expression Patterns Predict Gene Function in Mycobacteria. *Current Biology*
540 **30**: 3961-3971.e6 https://linkinghub.elsevier.com/retrieve/pii/S0960982220310952.
541 Accessed September 27, 2021.

542 Barford, D. (1996) Molecular mechanisms of the protein serine/threonine phosphatases.
543 *Trends Biochem Sci* **21**: 407–412.

544 Batt, S.M., Burke, C.E., Moorey, A.R., and Besra, G.S. (2020) Antibiotics and resistance:
545 the two-sided coin of the mycobacterial cell wall. *The Cell Surface* **6**: 100044
546 https://linkinghub.elsevier.com/retrieve/pii/S2468233020300116. Accessed October 1,
547 2020.

548 Betts, J.C., Lukey, P.T., Robb, L.C., McAdam, R.A., and Duncan, K. (2002) Evaluation
549 of a nutrient starvation model of Mycobacterium tuberculosis persistence by gene and
550 protein expression profiling. *Molecular Microbiology* **43**: 717–731
551 https://onlinelibrary.wiley.com/doi/abs/10.1046/j.1365-2958.2002.02779.x. Accessed
552 February 8, 2019.

553 Bhamidi, S., Shi, L., Chatterjee, D., Belisle, J.T., Crick, D.C., and McNeil, M.R. (2012)
554 A bioanalytical method to determine the cell wall composition of Mycobacterium
555 tuberculosis grown in vivo. *Analytical Biochemistry* **421**: 240–249
556 https://linkinghub.elsevier.com/retrieve/pii/S0003269711007123. Accessed February 5,
557 2020.

558 Bhaskara, G.B., Wong, M.M., and Verslues, P.E. (2019) The flip side of phospho-
559 signalling: Regulation of protein dephosphorylation and the protein phosphatase 2Cs.
560 *Plant Cell Environ* **42**: 2913–2930
561 https://onlinelibrary.wiley.com/doi/abs/10.1111/pce.13616. Accessed April 27, 2020.

562 Boitel, B., Ortiz-Lombardía, M., Durán, R., Pompeo, F., Cole, S.T., Cerveñansky, C., and
563 Alzari, P.M. (2003) PknB kinase activity is regulated by phosphorylation in two Thr
564 residues and dephosphorylation by PstP, the cognate phospho-Ser/Thr phosphatase, in
565 Mycobacterium tuberculosis: Mycobacterial serine/threonine kinase and phosphatase.
566 *Molecular Microbiology* **49**: 1493–1508 http://doi.wiley.com/10.1046/j.1365-
567 2958.2003.03657.x. Accessed February 6, 2019.

568 Boutte, C.C., Baer, C.E., Papavinasasundaram, K., Liu, W., Chase, M.R., Meniche, X., *et*
569 *al.* (2016) A cytoplasmic peptidoglycan amidase homologue controls mycobacterial cell
570 wall synthesis. *eLife* **5**: e14590 https://elifesciences.org/articles/14590. Accessed
571 September 19, 2019.

572 Bradshaw, N., Levdikov, V., Zimanyi, C., Gaudet, R., Wilkinson, A., and Losick, R.
573 (2017) A widespread family of serine/threonine protein phosphatases shares a common
574 regulatory switch with proteasomal proteases. *eLife* **6**.

575 Bradshaw, N., and Losick, R. (2015) Asymmetric division triggers cell-specific gene
576 expression through coupled capture and stabilization of a phosphatase. *eLife* **4**: e08145
577 https://elifesciences.org/articles/08145. Accessed September 19, 2019.

578 Carette, X., Platig, J., Young, D.C., Helmel, M., Young, A.T., Wang, Z., *et al.* (2018)
579 Multisystem Analysis of *Mycobacterium tuberculosis* Reveals Kinase-Dependent
580 Remodeling of the Pathogen-Environment Interface. *mBio* **9**
581 http://mbio.asm.org/lookup/doi/10.1128/mBio.02333-17. Accessed February 15, 2019.

582 Chopra, P., Singh, B., Singh, R., Vohra, R., Koul, A., Meena, L.S., *et al.* (2003)
583 Phosphoprotein phosphatase of Mycobacterium tuberculosis dephosphorylates serine-
584 threonine kinases PknA and PknB. *Biochem Biophys Res Commun* **311**: 112–120.

585 Cohen, P. (1989) The structure and regulation of protein phosphatases. *Annu Rev*
586 *Biochem* **58**: 453–508.

587 Cole, S.T., Brosch, R., Parkhill, J., Garnier, T., Churcher, C., Harris, D., *et al.* (1998)
588 Deciphering the biology of Mycobacterium tuberculosis from the complete genome
589 sequence. **396**: 27.

590 Cottin, V., Linden, A.V., and Riches, D.W.H. (1999) Phosphorylation of Tumor Necrosis
591 Factor Receptor CD120a (p55) by p42mapk/erk2 Induces Changes in Its Subcellular
592 Localization. 14.

593 Cunningham, A.F., and Spreadbury, C.L. (1998) Mycobacterial Stationary Phase Induced
594 by Low Oxygen Tension: Cell Wall Thickening and Localization of the 16-Kilodalton ␣-
595 Crystallin Homolog. *J BACTERIOL* **180**: 8.

596 DeJesus, M.A., Gerrick, E.R., Xu, W., Park, S.W., Long, J.E., Boutte, C.C., *et al.* (2017)
597 Comprehensive Essentiality Analysis of the *Mycobacterium tuberculosis* Genome via

598 Saturating Transposon Mutagenesis. *mBio* **8**: e02133-16, /mbio/8/1/e02133-16.atom
599 https://mbio.asm.org/content/8/1/e02133-16. Accessed August 1, 2020.

600 Doerks, T., Noort, V. van, Minguez, P., and Bork, P. (2012) Annotation of the M.
601 tuberculosis Hypothetical Orfeome: Adding Functional Information to More than Half of
602 the Uncharacterized Proteins. *PLoS ONE* **7**: e34302
603 https://dx.plos.org/10.1371/journal.pone.0034302. Accessed November 14, 2021.

604 Ducret, A., Quardokus, E.M., and Brun, Y.V. (2016) MicrobeJ, a tool for high throughput
605 bacterial cell detection and quantitative analysis. *Nature Microbiology* **1**: 16077
606 https://www.nature.com/articles/nmicrobiol201677. Accessed May 3, 2019.

607 Dulberger, C.L., Rubin, E.J., and Boutte, C.C. (2020) The mycobacterial cell envelope —
608 a moving target. *Nat Rev Microbiol* **18**: 47–59 http://www.nature.com/articles/s41579-
609 019-0273-7. Accessed May 20, 2021.

610 Durán, R., Villarino, A., Bellinzoni, M., Wehenkel, A., Fernandez, P., Boitel, B., *et al.*
611 (2005) Conserved autophosphorylation pattern in activation loops and juxtamembrane
612 regions of Mycobacterium tuberculosis Ser/Thr protein kinases. *Biochemical and*
613 *Biophysical Research Communications* **333**: 858–867
614 https://linkinghub.elsevier.com/retrieve/pii/S0006291X05011848. Accessed September
615 19, 2019.

616 Echenique, J., Kadioglu, A., Romao, S., Andrew, P.W., and Trombe, M.-C. (2004)
617 Protein Serine/Threonine Kinase StkP Positively Controls Virulence and Competence in
618 *Streptococcus pneumoniae*. *Infect Immun* **72**: 2434–2437
619 https://journals.asm.org/doi/10.1128/IAI.72.4.2434-2437.2004. Accessed November 15,
620 2021.

621 Fernandez, P., Saint-Joanis, B., Barilone, N., Jackson, M., Gicquel, B., Cole, S.T., and
622 Alzari, P.M. (2006) The Ser/Thr Protein Kinase PknB Is Essential for Sustaining
623 Mycobacterial Growth. *Journal of Bacteriology* **188**: 7778–7784
624 http://jb.asm.org/cgi/doi/10.1128/JB.00963-06. Accessed February 6, 2019.

625 Gee, C.L., Papavinasasundaram, K.G., Blair, S.R., Baer, C.E., Falick, A.M., King, D.S.,
626 *et al.* (2012) A Phosphorylated Pseudokinase Complex Controls Cell Wall Synthesis in
627 Mycobacteria. *Sci Signal* **5**: ra7–ra7 https://stke.sciencemag.org/content/5/208/ra7.
628 Accessed June 25, 2019.

629 Grundner, C., Gay, L.M., and Alber, T. (2005) *Mycobacterium tuberculosis*
630 serine/threonine kinases PknB, PknD, PknE, and PknF phosphorylate multiple FHA
631 domains. *Protein Sci* **14**: 1918–1921 http://doi.wiley.com/10.1110/ps.051413405.
632 Accessed September 19, 2019.

633 Gupta, M., Sajid, A., Arora, G., Tandon, V., and Singh, Y. (2009) Forkhead-associated
634 Domain-containing Protein Rv0019c and Polyketide-associated Protein PapA5, from
635 Substrates of Serine/Threonine Protein Kinase PknB to Interacting Proteins of
636 Mycobacterium tuberculosis. *Journal of Biological Chemistry* **284**: 34723–34734

637 https://linkinghub.elsevier.com/retrieve/pii/S0021925820375967. Accessed May 26,
638 2021.

639 Hannebelle, M.T.M., Ven, J.X.Y., Toniolo, C., Eskandarian, H.A., Vuaridel-Thurre, G.,
640 McKinney, J.D., and Fantner, G.E. (2020) A biphasic growth model for cell pole
641 elongation in mycobacteria. *Nat Commun* **11**: 452
642 http://www.nature.com/articles/s41467-019-14088-z. Accessed January 27, 2020.

643 Hett, E.C., and Rubin, E.J. (2008) Bacterial Growth and Cell Division: a Mycobacterial
644 Perspective. *Microbiology and Molecular Biology Reviews* **72**: 126–156
645 http://mmbr.asm.org/cgi/doi/10.1128/MMBR.00028-07. Accessed September 19, 2019.

646 Hoffmann, C., Leis, A., Niederweis, M., Plitzko, J.M., and Engelhardt, H. (2008)
647 Disclosure of the mycobacterial outer membrane: Cryo-electron tomography and vitreous
648 sections reveal the lipid bilayer structure. *Proceedings of the National Academy of*
649 *Sciences* **105**: 3963–3967 http://www.pnas.org/cgi/doi/10.1073/pnas.0709530105.
650 Accessed November 14, 2021.

651 Irmler, A., and Forchhammer, K. (2001) A PP2C-type phosphatase dephosphorylates the
652 PII signaling protein in the cyanobacterium Synechocystis PCC 6803. *Proceedings of the*
653 *National Academy of Sciences* **98**: 12978–12983
654 http://www.pnas.org/cgi/doi/10.1073/pnas.231254998. Accessed September 19, 2019.

655 Iswahyudi, Mukamolova, G.V., Straatman-Iwanowska, A.A., Allcock, N., Ajuh, P.,
656 Turapov, O., and O'Hare, H.M. (2019) Mycobacterial phosphatase PstP regulates global
657 serine threonine phosphorylation and cell division. *Sci Rep* **9**: 8337
658 http://www.nature.com/articles/s41598-019-44841-9. Accessed June 14, 2019.

659 Jani, C., Eoh, H., Lee, J., Hamasha, K., Sahana, M., Han, J.-S., *et al.* (2010) Regulation
660 of Polar Peptidoglycan Biosynthesis by Wag31 Phosphorylation in Mycobacteria. *BMC*
661 *Microbiol* **10**: 327 http://bmcmicrobiol.biomedcentral.com/articles/10.1186/1471-2180-
662 10-327. Accessed May 10, 2019.

663 Jarlier, V., and Nikaido, H. (1990) Permeability barrier to hydrophilic solutes in
664 Mycobacterium chelonei. *J Bacteriol* **172**: 1418–1423
665 https://journals.asm.org/doi/10.1128/jb.172.3.1418-1423.1990. Accessed November 14,
666 2021.

667 Jarlier, V., and Nikaido, H. (1994) Mycobacterial cell wall: Structure and role in natural
668 resistance to antibiotics. *FEMS Microbiology Letters* 11–18.

669 Juris, S.J., Rudolph, A.E., Huddler, D., Orth, K., and Dixon, J.E. (2000) A distinctive role
670 for the Yersinia protein kinase: Actin binding, kinase activation, and cytoskeleton
671 disruption. *Proceedings of the National Academy of Sciences* **97**: 9431–9436
672 http://www.pnas.org/cgi/doi/10.1073/pnas.170281997. Accessed November 15, 2021.

673 Kang, C.-M., Abbott, D.W., Park, S.T., Dascher, C.C., Cantley, L.C., and Husson, R.N.
674 (2005) The Mycobacterium tuberculosis serine/threonine kinases PknA and PknB:

675 substrate identification and regulation of cell shape. *Genes Dev* **19**: 1692–1704
676 https://www.ncbi.nlm.nih.gov/pmc/articles/PMC1176007/. Accessed July 15, 2019.

677 Kang, C.-M., Nyayapathy, S., Lee, J.-Y., Suh, J.-W., and Husson, R.N. (2008) Wag31, a
678 homologue of the cell division protein DivIVA, regulates growth, morphology and polar
679 cell wall synthesis in mycobacteria. *Microbiology* **154**: 725–735
680 http://mic.microbiologyresearch.org/content/journal/micro/10.1099/mic.0.2007/014076-
681 0. Accessed February 6, 2019.

682 Khan, S., Nagarajan, S.N., Parikh, A., Samantaray, S., Singh, A., Kumar, D., *et al.* (2010)
683 Phosphorylation of Enoyl-Acyl Carrier Protein Reductase InhA Impacts Mycobacterial
684 Growth and Survival. *Journal of Biological Chemistry* **285**: 37860–37871
685 http://www.jbc.org/lookup/doi/10.1074/jbc.M110.143131. Accessed February 6, 2019.

686 Kieser, K.J., Baranowski, C., Chao, M.C., Long, J.E., Sassetti, C.M., Waldor, M.K., *et al.*
687 (2015) Peptidoglycan synthesis in Mycobacterium tuberculosis is organized into
688 networks with varying drug susceptibility. *PNAS* **112**: 13087–13092
689 https://www.pnas.org/content/112/42/13087. Accessed March 12, 2019.

690 Kieser, K.J., and Rubin, E.J. (2014) How sisters grow apart: mycobacterial growth and
691 division. *Nature Reviews Microbiology* **12**: 550–562
692 http://www.nature.com/articles/nrmicro3299. Accessed February 6, 2019.

693 Kuru, E., Hughes, H.V., Brown, P.J., Hall, E., Tekkam, S., Cava, F., *et al.* (2012) In Situ
694 Probing of Newly Synthesized Peptidoglycan in Live Bacteria with Fluorescent D -
695 Amino Acids. *Angewandte Chemie International Edition* **51**: 12519–12523
696 http://doi.wiley.com/10.1002/anie.201206749. Accessed February 6, 2019.

697 Kusebauch, U., Ortega, C., Ollodart, A., Rogers, R.S., Sherman, D.R., Moritz, R.L., and
698 Grundner, C. (2014) Mycobacterium tuberculosis supports protein tyrosine
699 phosphorylation. *Proceedings of the National Academy of Sciences* **111**: 9265–9270
700 http://www.pnas.org/cgi/doi/10.1073/pnas.1323894111. Accessed November 15, 2021.

701 Liu, Y., Tan, S., Huang, L., Abramovitch, R.B., Rohde, K.H., Zimmerman, M.D., *et al.*
702 (2016) Immune activation of the host cell induces drug tolerance in *Mycobacterium*
703 *tuberculosis* both in vitro and in vivo. *J Exp Med* **213**: 809–825
704 http://www.jem.org/lookup/doi/10.1084/jem.20151248. Accessed May 9, 2019.

705 Lu, G., and Wang, Y. (2008) FUNCTIONAL DIVERSITY OF MAMMALIAN TYPE
706 2C PROTEIN PHOSPHATASE ISOFORMS: NEW TALES FROM AN OLD FAMILY:
707 Function of PP2C isoforms. *Clinical and Experimental Pharmacology and Physiology*
708 **35**: 107–112 https://onlinelibrary.wiley.com/doi/10.1111/j.1440-1681.2007.04843.x.
709 Accessed November 19, 2021.

710 Marquardt, J.L., Siegele, D.A., Kolter, R., and Walsh, C.T. (1992) Cloning and
711 sequencing of Escherichia coli murZ and purification of its product, a UDP-N-
712 acetylglucosamine enolpyruvyl transferase. *J Bacteriol* **174**: 5748–5752

713 https://journals.asm.org/doi/10.1128/jb.174.17.5748-5752.1992. Accessed November 15,
714 2021.

715 Marrakchi, H., Lanéelle, M.-A., and Daffé, M. (2014) Mycolic Acids: Structures,
716 Biosynthesis, and Beyond. *Chemistry & Biology* **21**: 67–85
717 http://www.sciencedirect.com/science/article/pii/S1074552113004201. Accessed
718 February 6, 2019.

719 Molle, V., Brown, A.K., Besra, G.S., Cozzone, A.J., and Kremer, L. (2006) The
720 Condensing Activities of the Mycobacterium tuberculosis Type II Fatty Acid Synthase
721 Are Differentially Regulated by Phosphorylation. *Journal of Biological Chemistry* **281**:
722 30094–30103 https://linkinghub.elsevier.com/retrieve/pii/S0021925819339158. Accessed
723 May 26, 2021.

724 Molle, V., and Kremer, L. (2010) Division and cell envelope regulation by Ser/Thr
725 phosphorylation: *Mycobacterium* shows the way. *Molecular Microbiology* **75**: 1064–
726 1077 http://doi.wiley.com/10.1111/j.1365-2958.2009.07041.x. Accessed February 6,
727 2019.

728 Mougous, J.D., Gifford, C.A., Ramsdell, T.L., and Mekalanos, J.J. (2007) Threonine
729 phosphorylation post-translationally regulates protein secretion in Pseudomonas
730 aeruginosa. *Nat Cell Biol* **9**: 797–803 http://www.nature.com/articles/ncb1605. Accessed
731 November 19, 2021.

732 Nguyen, L. (2016) Antibiotic resistance mechanisms in M. tuberculosis: an update. *Arch*
733 *Toxicol* **90**: 1585–1604 http://link.springer.com/10.1007/s00204-016-1727-6. Accessed
734 September 19, 2019.

735 Pashley, C.A., and Parish, T. (2003) Efficient switching of mycobacteriophage L5-based
736 integrating plasmids in *Mycobacterium tuberculosis*. *FEMS Microbiology Letters* **229**:
737 211–215 https://academic.oup.com/femsle/article-lookup/doi/10.1016/S0378-
738 1097(03)00823-1. Accessed February 6, 2019.

739 Prisic, S., Dankwa, S., Schwartz, D., Chou, M.F., Locasale, J.W., Kang, C.-M., *et al.*
740 (2010) Extensive phosphorylation with overlapping specificity by Mycobacterium
741 tuberculosis serine/ threonine protein kinases. *Proceedings of the National Academy of*
742 *Sciences* **107**: 7521–7526.

743 Prisic, S., and Husson, R.N. (2014) Mycobacterium tuberculosis Serine/Threonine
744 Protein Kinases. *Microbiology Spectrum* **2**
745 http://www.asmscience.org/content/journal/microbiolspec/10.1128/microbiolspec.MGM2
746 -0006-2013. Accessed February 6, 2019.

747 Pullen, K.E., Ng, H.-L., Sung, P.-Y., Good, M.C., Smith, S.M., and Alber, T. (2004) An
748 Alternate Conformation and a Third Metal in PstP/Ppp, the M. tuberculosis PP2C-Family
749 Ser/Thr Protein Phosphatase. *Structure* **12**: 1947–1954
750 https://linkinghub.elsevier.com/retrieve/pii/S096921260400334X. Accessed May 26,
751 2021.

752 Roumestand, C., Leiba, J., Galophe, N., Margeat, E., Padilla, A., Bessin, Y., *et al.* (2011)
753 Structural Insight into the Mycobacterium tuberculosis Rv0020c Protein and Its
754 Interaction with the PknB Kinase. *Structure* **19**: 1525–1534
755 http://www.sciencedirect.com/science/article/pii/S096921261100253X. Accessed March
756 27, 2019.

757 Sajid, A., Arora, G., Gupta, M., Upadhyay, S., Nandicoori, V.K., and Singh, Y. (2011)
758 Phosphorylation of Mycobacterium tuberculosis Ser/Thr Phosphatase by PknA and PknB.
759 *PLoS ONE* **6**: e17871 https://dx.plos.org/10.1371/journal.pone.0017871. Accessed
760 December 9, 2021.

761 Sarathy, J., Dartois, V., Dick, T., and Gengenbacher, M. (2013) Reduced Drug Uptake in
762 Phenotypically Resistant Nutrient-Starved Nonreplicating Mycobacterium tuberculosis.
763 *Antimicrobial Agents and Chemotherapy* **57**: 1648–1653
764 http://aac.asm.org/lookup/doi/10.1128/AAC.02202-12. Accessed February 6, 2019.

765 Sarathy, J.P., Via, L.E., Weiner, D., Blanc, L., Boshoff, H., Eugenin, E.A., *et al.* (2017)
766 Extreme Drug Tolerance of *Mycobacterium tuberculosis* in Caseum. *Antimicrobial*
767 *Agents and Chemotherapy* **62** http://aac.asm.org/lookup/doi/10.1128/AAC.02266-17.
768 Accessed February 6, 2019.

769 Sassetti, C.M., and Rubin, E.J. (2003) Genetic requirements for mycobacterial survival
770 during infection. *Proceedings of the National Academy of Sciences* **100**: 12989–12994
771 http://www.pnas.org/cgi/doi/10.1073/pnas.2134250100. Accessed August 1, 2020.

772 Shamma, F., Quintanilla, S., Bandekar, A., Sassetti, C., and Boutte, C. (2021)
773 Phosphorylation on PstP Regulates Cell Wall Metabolism and Antibiotic Tolerance in
774 Mycobacterium smegmatis. *Journal of Bacteriology* **203**: e00563-20.

775 Sharma, A.K., Arora, D., Singh, L.K., Gangwal, A., Sajid, A., Molle, V., *et al.* (2016)
776 Serine/Threonine Protein Phosphatase PstP of *Mycobacterium tuberculosis* Is Necessary
777 for Accurate Cell Division and Survival of Pathogen. *Journal of Biological Chemistry*
778 **291**: 24215–24230 http://www.jbc.org/lookup/doi/10.1074/jbc.M116.754531. Accessed
779 February 6, 2019.

780 Sharma, K., Gupta, M., Krupa, A., Srinivasan, N., and Singh, Y. (2006) EmbR, a
781 regulatory protein with ATPase activity, is a substrate of multiple serine/threonine
782 kinases and phosphatase in *Mycobacterium tuberculosis*. *FEBS Journal* **273**: 2711–2721
783 http://doi.wiley.com/10.1111/j.1742-4658.2006.05289.x. Accessed May 26, 2021.

784 Slama, N., Leiba, J., Eynard, N., Daffé, M., Kremer, L., Quémard, A., and Molle, V.
785 (2011) Negative regulation by Ser/Thr phosphorylation of HadAB and HadBC
786 dehydratases from Mycobacterium tuberculosis type II fatty acid synthase system.
787 *Biochemical and Biophysical Research Communications* **412**: 401–406
788 https://linkinghub.elsevier.com/retrieve/pii/S0006291X11012770. Accessed March 31,
789 2019.

790 Thakur, M., and Chakraborti, P.K. (2006) GTPase Activity of Mycobacterial FtsZ Is
791 Impaired Due to Its Transphosphorylation by the Eukaryotic-type Ser/Thr Kinase, PknA.
792 *J Biol Chem* **281**: 40107–40113
793 http://www.jbc.org/lookup/doi/10.1074/jbc.M607216200. Accessed May 8, 2019.

794 Turapov, O., Forti, F., Kadhim, B., Ghisotti, D., Sassine, J., Straatman-Iwanowska, A., *et*
795 *al.* (2018) Two Faces of CwlM, an Essential PknB Substrate, in Mycobacterium
796 tuberculosis. *Cell Rep* **25**: 57-67.e5
797 https://www.ncbi.nlm.nih.gov/pmc/articles/PMC6180346/. Accessed July 22, 2020.

798 Veyron-Churlet, R., Zanella-Cléon, I., Cohen-Gonsaud, M., Molle, V., and Kremer, L.
799 (2010) Phosphorylation of the *Mycobacterium tuberculosis* β-Ketoacyl-Acyl Carrier
800 Protein Reductase MabA Regulates Mycolic Acid Biosynthesis. *Journal of Biological*
801 *Chemistry* **285**: 12714–12725 http://www.jbc.org/lookup/doi/10.1074/jbc.M110.105189.
802 Accessed February 6, 2019.

803 Vijay, K., Brody, M.S., Fredlund, E., and Price, C.W. (2000) A PP2C phosphatase
804 containing a PAS domain is required to convey signals of energy stress to the sB
805 transcription factor of Bacillus subtilis. *Molecular Microbiology* 9.

806 Vilchèze, C., Molle, V., Carrère-Kremer, S., Leiba, J., Mourey, L., Shenai, S., *et al.*
807 (2014) Phosphorylation of KasB Regulates Virulence and Acid-Fastness in
808 Mycobacterium tuberculosis. *PLoS Pathogens* **10**: e1004115
809 http://dx.plos.org/10.1371/journal.ppat.1004115. Accessed February 6, 2019.

810 Viswanathan, G., Joshi, S.V., Sridhar, A., Dutta, S., and Raghunand, T.R. (2015)
811 Identifying novel mycobacterial stress associated genes using a random mutagenesis
812 screen in Mycobacterium smegmatis. *Gene* **574**: 20–27
813 https://linkinghub.elsevier.com/retrieve/pii/S037811191500904X. Accessed November
814 11, 2021.

815 Viswanathan, G., Yadav, S., Joshi, S.V., and Raghunand, T.R. (2016) Insights into the
816 function of FhaA, a cell-division associated protein in mycobacteria. *FEMS Microbiology*
817 *Letters* fnw294 https://academic.oup.com/femsle/article-
818 lookup/doi/10.1093/femsle/fnw294. Accessed February 6, 2019.

819 Viswanathan, G., Yadav, S., and Raghunand, T.R. (2017) Identification of Mycobacterial
820 Genes Involved in Antibiotic Sensitivity: Implications for the Treatment of Tuberculosis
821 with β-Lactam-Containing Regimens. *Antimicrobial Agents and Chemotherapy* **61**
822 http://aac.asm.org/lookup/doi/10.1128/AAC.00425-17. Accessed February 6, 2019.

823 Wang, J., Li, C., Yang, H., Mushegian, A., and Jin, S. (1998) A Novel Serine/Threonine
824 Protein Kinase Homologue of *Pseudomonas aeruginosa* Is Specifically Inducible within
825 the Host Infection Site and Is Required for Full Virulence in Neutropenic Mice. *J*
826 *Bacteriol* **180**: 6764–6768 https://journals.asm.org/doi/10.1128/JB.180.24.6764-
827 6768.1998. Accessed November 15, 2021.

828 World Health Organization (2021) *Global tuberculosis report 2021*. World Health
829 Organization, Geneva. https://apps.who.int/iris/handle/10665/346387. Accessed
830 November 14, 2021.

831 Xie, Z., Siddiqi, N., and Rubin, E.J. (2005) Differential Antibiotic Susceptibilities of
832 Starved Mycobacterium tuberculosis Isolates. *Antimicrobial Agents and Chemotherapy*
833 **49**: 4778–4780 http://aac.asm.org/cgi/doi/10.1128/AAC.49.11.4778-4780.2005.
834 Accessed February 6, 2019.

835

836 **PstP T137 paper 2022 Figures**
837

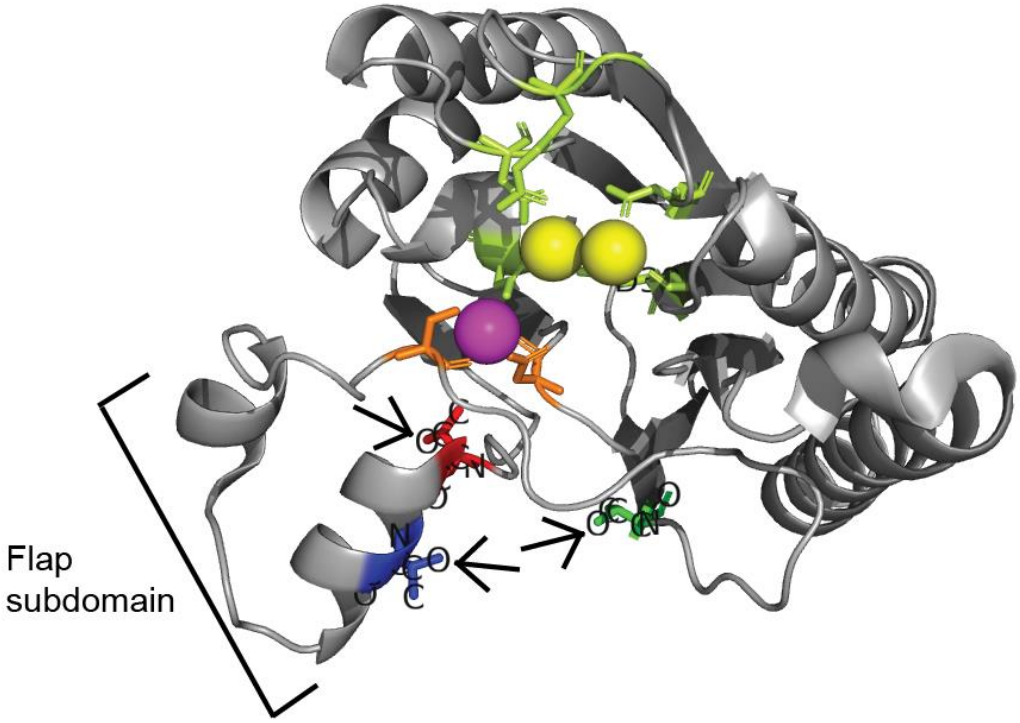

838
839
840
841 **Figure 1 Phosphorylation sites are not near the active site in PstP**

842 Schematic of the crystal structure of PstP from *M. tuberculosis* ($PstP_{Mtb}$WT)
843 (Pullen *et al.*, 2004) (PDB code 1TXO) showing the conserved threonines (T)
844 which are phosphorylated by the kinases PknA and PknB (Sajid *et al.*, 2011).
845 Highlighted on the structure are: red - $PstP_{Mtb}$T137 (PstPT134 in $PstP_{Msmeg}$); blue
846 - $PstP_{Mtb}$T141 (PstPT138 in $PstP_{Msmeg}$); green - $PstP_{Mtb}$T174 (PstPT171 in
847 $PstP_{Msmeg}$); yellow - Mn^{2+} present at the conserved two-metal center typically
848 seen in the PP2C subfamily of protein Serine/Threonine phosphatases, which
849 are part of the active site core; pink - the unique third Mn^{2+} ion bound in the
850 catalytic core of $PstP_{Mtb}$ but not present in the human PP2Cα which sits in a
851 groove created by the flap subdomain next to the active site; orange - Ser60 and
852 Asp118 that act as ligands for the third Mn ion; lime green - residues of the
853 catalytic sites surrounding the two-metal center. Arrows point to position of the
854 OH-groups on T137, T141 and T174 that are phosphorylated.

855

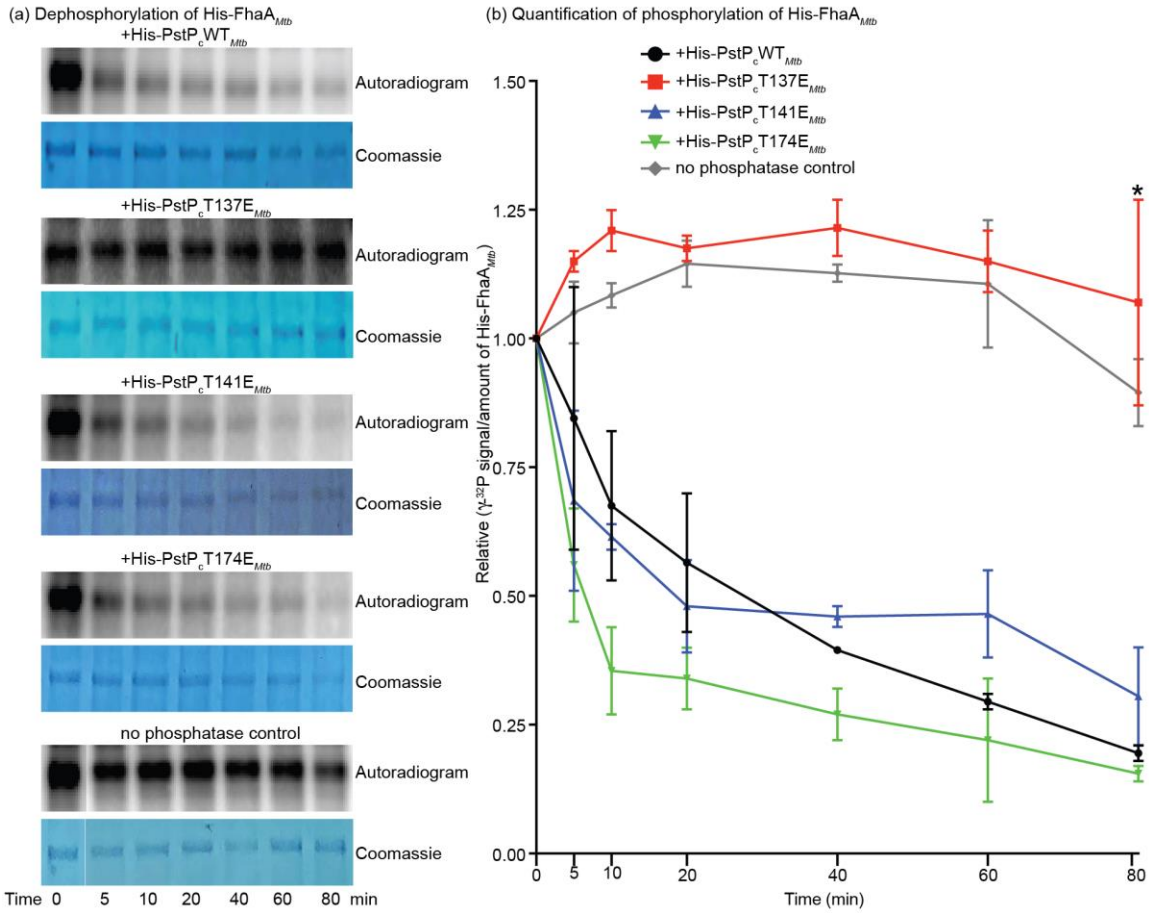

FIGURE 2 Dephosphorylation of FhaA by PstP and phospho-mimetic isoforms

(a) Autoradiograms and corresponding Coomassie stained SDS-gels of *in vitro* phosphatase assays performed with ATP-[γ-^{32}P]-phosphorylated His-FhaA$_{Mtb}$ and His-PstP$_c$WT$_{Mtb}$ (first panel), His-PstP$_c$137E$_{Mtb}$ (second panel), His-PstP$_c$T141E$_{Mtb}$ (third panel), His-PstP$_c$T174E$_{Mtb}$ (fourth panel) and no phosphatase control reaction (bottom panel). One set of representative images for each assay is shown here from two individual assays performed with individually purified batches of phosphatases.

(b) Quantification of relative intensities of [γ-^{32}P] on His-FhaA$_{Mtb}$ on autoradiogram over amount of His-FhaA$_{Mtb}$ on the SDS-gel. P values were calculated using two-tailed unpaired t-test.

P-values of T137E at 0 min *vs.* T137E 80 min =0.7598, WT *vs.* T137E at 80 min= 0.0487, WT *vs.* T141E at 80 min =0.3712, WT *vs.* T174E at 80 min=0.2000. The error bars represent standard error of mean.

873

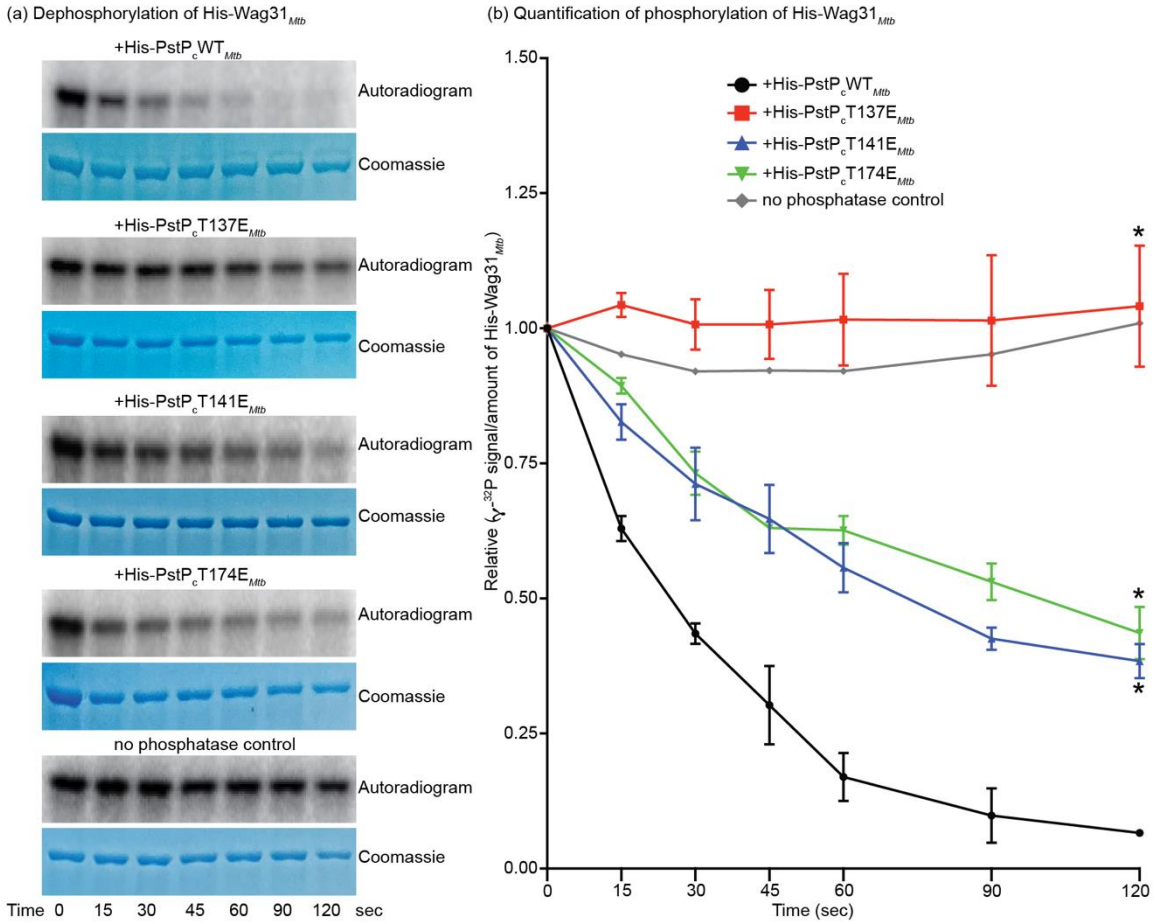

874
875
876 **FIGURE 3 Dephosphorylation of Wag31*Mtb* by PstP and phospho-mimetic**
877 **isoforms**
878

879 (a) Autoradiograms and their respective Coomassie stained SDS-gels of *in vitro*
880 phosphatase assays performed with ATP-[γ-^{32}P]-phosphorylated His-Wag31$_{Mtb}$
881 and His-PstP$_c$WT$_{Mtb}$ (first panel), His-PstP$_c$WT$_{Mtb}$ (second panel), His-
882 PstP$_c$T141E$_{Mtb}$ (third panel), His-PstP$_c$T174E$_{Mtb}$ (fourth panel) and no
883 phosphatase control reaction (bottom panel). One set of representative images
884 for each reaction is shown here from two individual assays performed with
885 individually purified batches of phosphatases.

886 (b) Quantification of relative intensities of [γ-^{32}P] on His-Wag31$_{Mtb}$ on
887 autoradiogram over amount of His-Wag31$_{Mtb}$ on the SDS-gel. P values were
888 calculated using two-tailed unpaired t-test.

889 P-values of T137E at 0 sec *vs.* 15 sec = 0. 0.1947 and 0 sec *vs.* 120sec= 0.7493,
890 WT *vs.* T137E at 120 sec= 0.0130, WT *vs.* T141E at 120 sec =0.0106 and WT
891 *vs.* T174E at 120 sec = 0.170. The error bars represent standard error of mean.

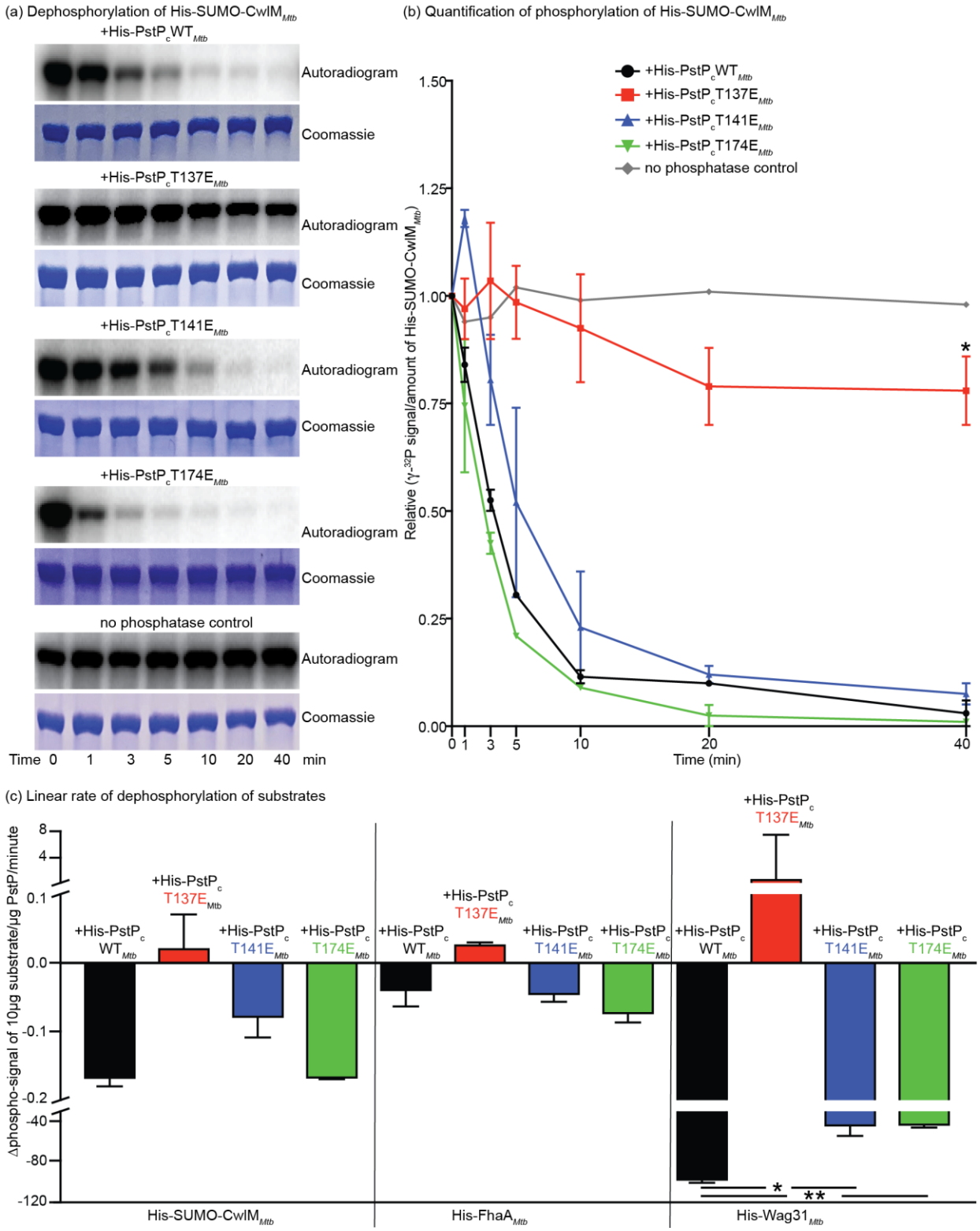

892

893
894 **FIGURE 4 Dephosphorylation of CwlM$_{Mtb}$ by PstP$_{Mtb}$ its phospho-mimetic**
895 **isoforms and linear rate of dephosphorylation of CwlM$_{Mtb}$, FhaA$_{Mtb}$ and**
896 **Wag31$_{Mtb}$**

897 (a) Autoradiograms and their respective Coomassie stained SDS-gels of *in vitro*
898 phosphatase assays performed with ATP-[γ-^{32}P]-phosphorylated His-SUMO-
899 CwlM$_{Mtb}$ and His-PstP$_c$WT$_{Mtb}$ (first panel), His-PstP$_c$WT$_{Mtb}$ (second panel), His-
900 PstP$_c$T141E$_{Mtb}$ (third panel), His-PstP$_c$T174E$_{Mtb}$ (fourth panel) and no
901 phosphatase control reaction (bottom panel). One set of representative images
902 for each reaction is shown here from two individual assays performed with
903 individually purified batches of phosphatases.

904 (b) Quantification of relative intensities of [γ-^{32}P] on His-SUMO-CwlM$_{Mtb}$ on
905 autoradiogram over amount of His-SUMO-CwlM$_{Mtb}$ on the SDS-gel. P values
906 were calculated using two-tailed unpaired t-test. P-values of T137E at 0 min *vs.*
907 40 min= 0.1107, WT *vs*. T137E at 40 min= 0.0127, WT *vs*. T141E at 40
908 min=0.3683 and WT *vs*. T174E at 40 min= 0.5918. The error bars represent
909 standard error of mean.

910 (c) Quantification of linear rate of change in [γ-^{32}P] signal on 10µg of His-SUMO-
911 CwlM$_{Mtb}$, His-FhaA$_{Mtb}$ and His-Wag31$_{Mtb}$ in presence of His-PstP$_c$WT$_{Mtb}$ and its
912 phospho-mimetic mutants per minute. P values were calculated using two-tailed
913 unpaired t-test. **, P value = 0.0026 and *, P value 0306. The error bars
914 represent standard error of mean.

915

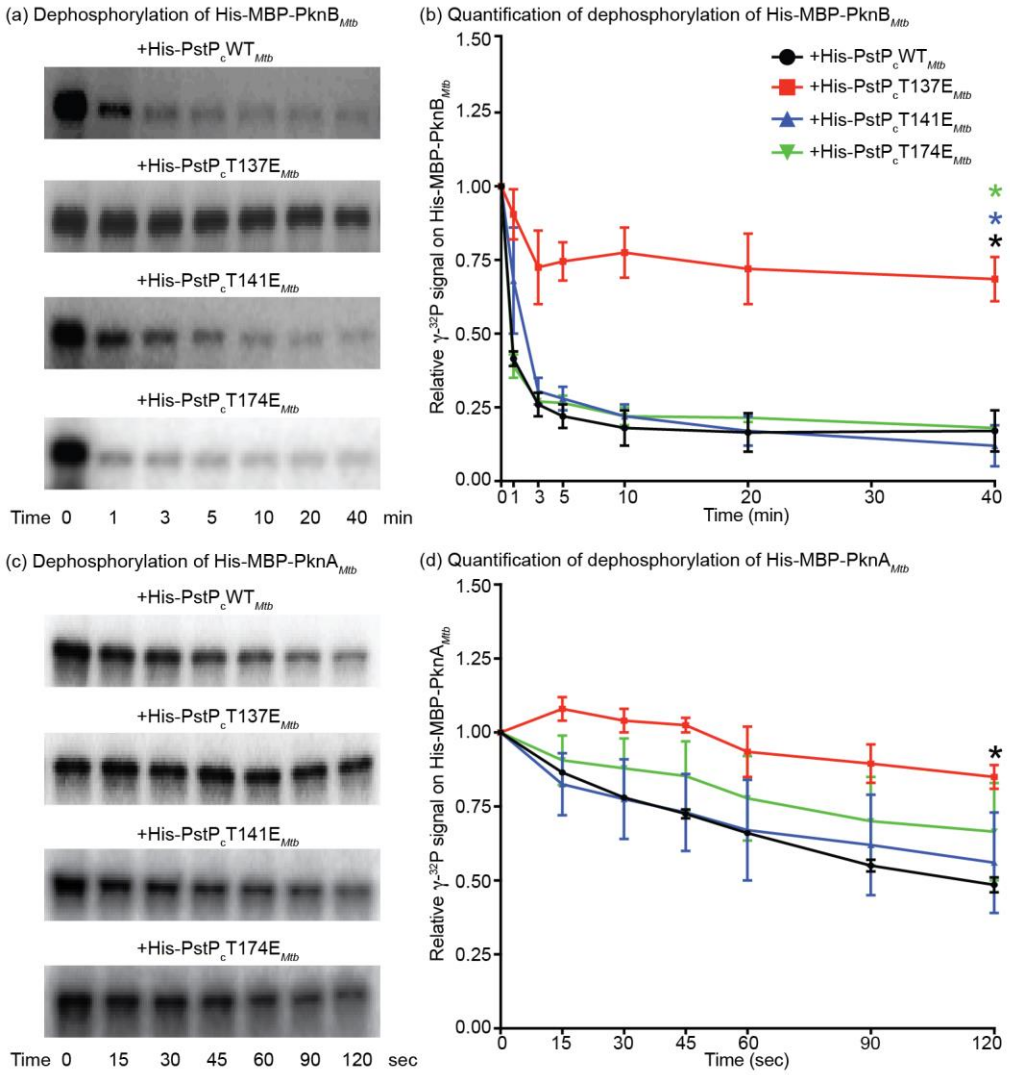

FIGURE 5 Dephosphorylation of PknB$_{Mtb}$ and PknA by PstPWT$_{Mtb}$ and its phospho-mimetic variants

(a) Autoradiograms showing [γ-^{32}P]-phospho-signals on His-MBP-PknB$_{Mtb}$ in the *in vitro* phosphatase assays with His-SUMO-CwlM$_{Mtb}$ and His-PstP$_c$WT$_{Mtb}$ (first panel), His-PstP$_c$WT$_{Mtb}$ (second panel), His-PstP$_c$T141E$_{Mtb}$ (third panel) and His-PstP$_c$T174E$_{Mtb}$ (fourth panel), where His-MBP-PknB$_{Mtb}$ was used to phosphorylate His-SUMO-CwlM$_{Mtb}$. One set of representative images for each reaction is shown here from two individual assays performed with individually purified batches of phosphatases.

(b) Quantification of relative intensities of [γ-^{32}P] on His-MBP-PknB$_{Mtb}$ on autoradiogram. P values were calculated using two-tailed unpaired t-test. P value of T137E at 0 min *vs.* 40 min= 0.0523. *, P value= 0.0375 (WT *vs.*T137E at 40 min); *, P value=0.0314 (T141E *vs.*T137E at 40 min); *, P value= 0.0217 (T174E *vs.*T137E at 40 min). The error bars represent standard error of mean.

931 (c) Autoradiograms showing [γ-^{32}P]-phospho-signals on His-MBP-PknA$_{Mtb}$ in the *in*
932 *vitro* phosphatase assays with His-Wag31$_{Mtb}$ and His-PstP$_c$WT$_{Mtb}$ (first panel),
933 His-PstP$_c$WT$_{Mtb}$ (second panel), His-PstP$_c$T141E$_{Mtb}$ (third panel) and His-
934 PstP$_c$T174E$_{Mtb}$ (fourth panel), where His-Wag31$_{Mtb}$ was first phosphorylated with
935 His-MBP-PknA$_{Mtb}$. One set of representative images for each reaction is shown
936 here from two individual assays performed with individually purified batches of
937 phosphatases.

938 (d) Quantification of relative intensities of [γ-^{32}P] on His-MBP-PknA$_{Mtb}$ on
939 autoradiogram. P values were calculated using two-tailed unpaired t-test. P value
940 of T137E at 0 sec *vs.* 120 sec= 0.0643. *, P value= 0.0163 (WT *vs*. T137E at 120
941 sec). The error bars represent standard error of mean.

942

943
944

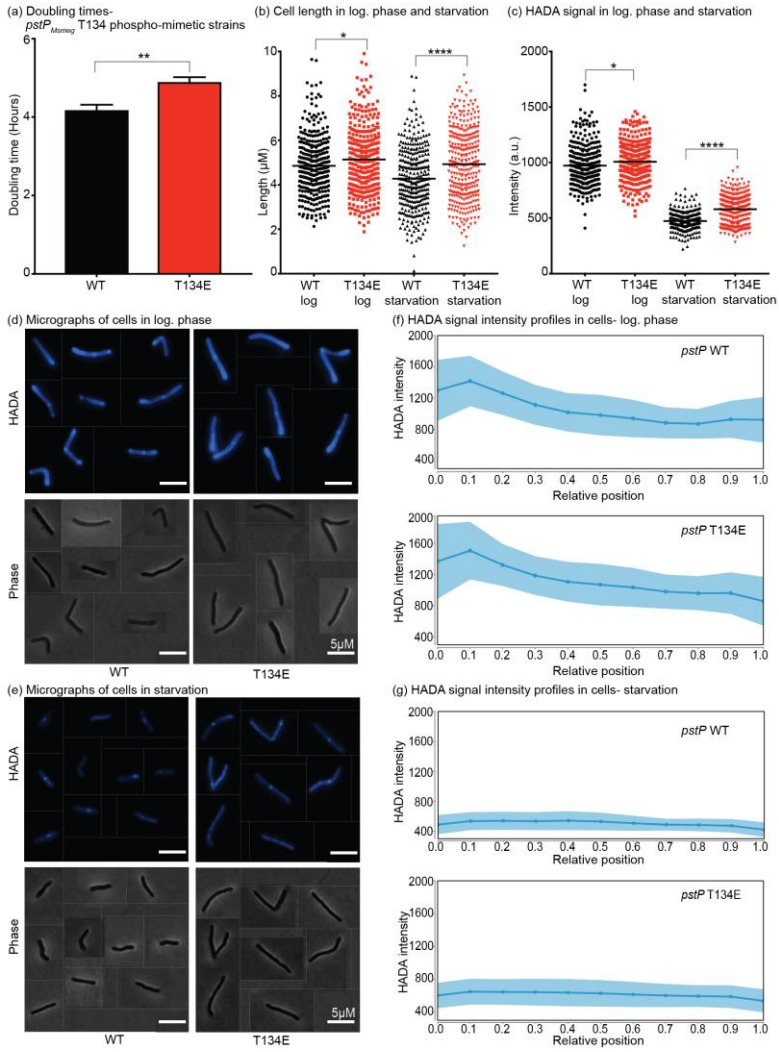

945
946 **Figure 6 The phosphosite on T134 on PstP$_{Msmeg}$ affects PG metabolism**

947 (a) Doubling times of *Msmeg* strains carrying the $pstP_{Msmeg}$ WT and the phospho-
948 mimetic T134E alleles. Each bar represents the mean of individual average
949 doubling times of three biological replicates of each genotype from two different
950 experiments on different dates. The error bars represent mean with standard
951 deviation. **, P value= 0.0026.

952 (b) Quantification of cell lengths of isogenic $pstP_{Msmeg}$ allele strains (WT and
953 T134E) grown in 7H9 in log. phase and starved in PBS with Tween80. At least
954 100 cells from each of three biological replicates were quantified. P values were
955 calculated by unpaired t-test. *, P value = 0.0122, ****, P value= 0.000000031.

956 (c) Quantification of mean intensities of HADA of $pstP_{Msmeg}$ allele strains (WT and
957 T134E) grown in 7H9 in log. phase and starved in PBS with Tween80. Cells were
958 stained after 15 minutes of starvation and washed and fixed after another 15
959 minutes (starved for a total of 30 minutes). At least 100 cells from each of three
960 biological replicates were quantified. P values were calculated by unpaired t-test.
961 *, P value = 0.0109, ****, P value= <0.000000000000001.

962 (d) and (e) Representative HADA and phase images of cells from $pstP_{Msmeg}$ allele
963 strains (WT and T134E) grown in 7H9 in log. phase (d) and after 30 minutes of
964 starvation in PBS with Tween80 (e).

965 (f) and (g) Intensity profiles of HADA signals in cells of $pstP_{Msmeg}$ allele strains
966 (WT and T134E) in log. phase (f) and after starving for 30 minutes in PBS
967 supplemented with Tween80 (g). The shaded regions denote standard deviations
968 and the solid lines represent the mean intensity values. Signal intensities from at
969 least 110 cells from each of three biological replicates of every $pstP_{Msmeg}$ allelic
970 variant genotype were quantified and used to analyze the signal profiles in
971 MicrobeJ. 0 to 1 on the X-axes represent cells from the old pole to the new pole,
972 respectively.

973

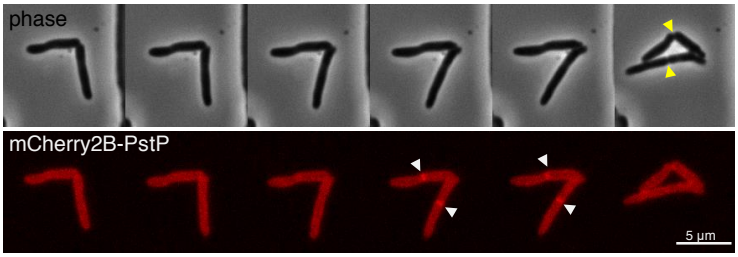

974

975 **Figure 7 Localization of PstPWT$_{Msmeg}$**

976 *Msmeg* cells expressing mCherry2B-PstP were imaged over time in a CellAsic
977 Microfluidic device at 15-minute intervals. Intensity is seen at the midcell (white

978 arrows) for several frames before cell separation can be visualized by phase
979 contrast microscopy (yellow arrows).

980

981

982

983

984 **Supplemental Figures:**

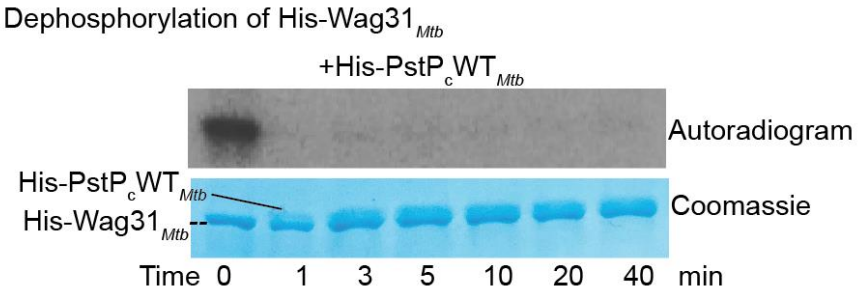

985
986

987 **Supplementary Figure S1: Dephosphorylation of His-Wag31*Mtb* by His-**
988 **PstP$_c$WT*Mtb*.** Autoradiogram and the respective Coomassie stained SDS-gel of *in*
989 *vitro* phosphatase assays performed with ATP-[γ-^{32}P]-phosphorylated His-
990 Wag31$_{Mtb}$ and His-PstP$_c$WT$_{Mtb}$. Ten times more substrate than the phosphatase
991 was used in the assay.

992

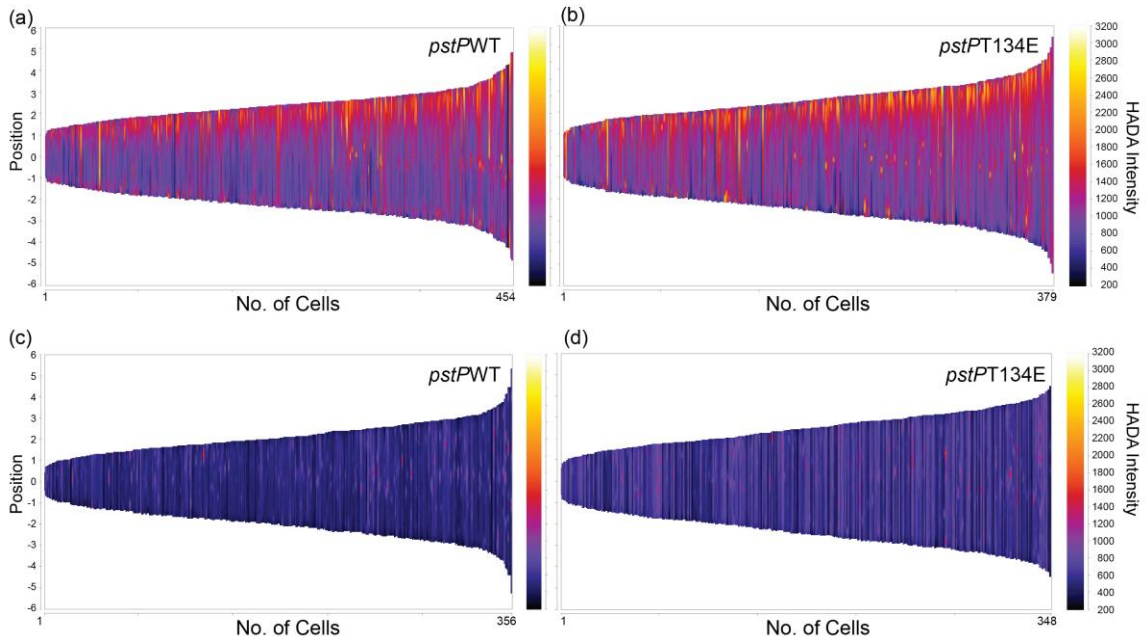

Supplementary Figure S2: Demographic profiles of HADA signal intensity in *pstP*$_{Msmeg}$ strains in growth and starvation. (a) and (b) Demographs showing intensities of the fluorescent dye HADA signal in individual cells from *pstP*$_{Msmeg}$WT allele strains (a) and *pstP*$_{Msmeg}$T134E allele strains (b) in log. phase. (c) and (d) Demographs showing intensities of the fluorescent dye HADA signal in individual cells from *pstP*$_{Msmeg}$WT allele strains (c) and *pstP*$_{Msmeg}$T134E allele strains (d) starved in PBS with Tween80 for a total time period of 30 minutes.

Biological triplicates of each *pstP*$_{Msmeg}$ allelic variant were analyzed. Signal intensities from at least 340 cells from each *pstP* allelic variant (at least 100 cells from each biological triplicate of each genotype) in log. phase and starvation were plotted in the demographs.